Exploring river–aquifer interactions and hydrological system response using baseflow separation, impulse response modelling and time series analysis in three temperate lowland catchments

Min Lu[1,2], Bart Rogiers[1], Koen Beerten[1], Matej Gedeon[1], Marijke Huysmans[2,3]

[1]Institute for Environment, Health and Safety, Belgian Nuclear Research Centre, Mol, 2400, Belgium
[2]Department of Earth and Environmental Sciences, KU Leuven, Leuven, 3001, Belgium
[3]Department of Hydrology and Hydraulic Engineering, Vrije Universiteit Brussel, Brussels, 1050, Belgium

Correspondence to: Min Lu (mlu@sckcen.be)

Abstract. Lowland rivers and shallow aquifers are closely coupled and their interactions are crucial for maintaining healthy stream ecological functions. To explore river–aquifer interactions and lowland hydrological system in three Belgian catchments, we apply a combined approach of baseflow separation, impulse response modelling and time series analysis over a 30–year study period at the catchment scale. Baseflow from hydrograph separation shows that the three catchments are groundwater-dominated. The recursive digital filter methods generate a smoother baseflow time series than the graphical methods. Impulse response modelling is applied with a two–step procedure. The first step of groundwater level response modelling shows that groundwater level in shallow aquifers reacts fast to the system input, with most of the wells reaching their peak response during the first day. There is an overall trend of faster response time and higher response magnitude in the wet (October–March) than the dry (April–September) periods. The second step of groundwater inflow response modelling shows that the system response is also fast and that simulated groundwater inflow can capture some variations but not the peaks of the separated baseflow time series. The time series analysis indicates that groundwater discharge to rivers is likely following groundwater level time series characteristics, with strong trend and seasonal strengths, in contract to the stream flow which exhibits a weak trend and seasonality. The impulse response modelling approach from the groundwater flow perspective can be an alternative method to estimate the groundwater inflow to rivers, since it considers the physical connection between river and aquifer to a certain extent. Further research is recommended to improve the simulation, such as giving more weight to wells close to the river and adding more drainage dynamics to the model input.

1 Introduction

In riverine environments, stream flow quantity and water quality are often largely influenced by groundwater (GW) via flow and solute exchange. River–aquifer interactions impact the stream ecological functions since a lot of vegetation types are highly dependent on a healthy flow regime and nutrient level. Their interactions, on the other hand, are directly linked with and influenced by changes in climate, land use, land cover, water management policies, and other human activities. Emerging hydrological stresses, such as observed record droughts in recent decades in Europe, have already resulted in low stream discharge, stream stage and groundwater level (Fu et al., 2020; Hänsel et al., 2019; Spinoni et al., 2017; Laaha et al., 2017). Therefore, understanding river–groundwater interactions and exploring their temporal evolution are of crucial importance, and can provide insights and assistance for future environmental management decisions to minimize the potential adverse effects and maintain a healthy hydro-ecological balance.

Lowland catchments in temperate regions are characterized by flat topographies and shallow groundwater tables. Rivers and groundwater in these catchments are closely coupled and influenced by climatic drivers, such as precipitation (van Walsum et al., 2002). Previous studies conducted on lowland river–aquifer interactions have their distinctive objectives and applied methodologies. For example, to quantify the exchange fluxes, there are hydraulic or heat tracer approaches (Krause et al., 2012), or event-based hydrochemical and isotopic tracer methods (Poulsen et al., 2015). Process modelling approaches are often used to simulate the river–aquifer interactions. The ubiquitous, and open source, numerical groundwater modelling code MODFLOW has for instance several options for two-way surface water and groundwater interactions (Niswonger and Prudic, 2005; Di Ciacca et al., 2019; Nützmann et al., 2013). More fully integrated models, taking into account the physics of the surface and subsurface domains, such as HydroGeoSphere (Alaghmand et al., 2016), exist as well. Comprehensive reviews on approaches and applications for better understanding river–groundwater interactions can be found in recent papers and books (Brunner et al., 2017; Cushman and Tartakovsky, 2016; Barthel and Banzhaf, 2016).

In Belgium, research projects with a focus on river–aquifer interactions have been intensively carried out in the Aa river, a typical Flemish lowland river, using various methods, such as heat tracer, river bed hydraulic conductivity measurements and numerical modelling approaches (Anibas et al., 2009, 2011, 2015, 2017; Ghysels et al., 2018, 2021; Schneidewind et al., 2016). However, these applications are limited to relatively small spatial scale studies, e.g. at the point scale or a short river segment, and difficult to upscale due to the complexity of small-scale heterogeneity in river bed materials and river morphology (Ghysels et al., 2018). The research periods in these projects cover relatively short temporal scales, where field data were collected on a few days at chosen seasons (summer and winter) or for a maximum of a few years. Very few studies have assessed the river–aquifer interactions at a larger spatial and temporal scale in Belgian lowland catchments, using methods other than baseflow separation techniques (Zomlot et al., 2015; Batelaan and De Smedt, 2007). Furthermore, there is little research done in the selected lowland catchments (see Sect. 2) with respect to river–aquifer interaction studies, the outcome of which is important

for assessing the potential for groundwater-sensitive species in the framework of ecological studies and management practices in these sites.

60

In this study, we present a combined approach of baseflow separation, impulse response modelling and time series analysis to gain insights into the hydrological system and the interactions between rivers and shallow aquifers over a 30-year period in three temperate lowland catchments. Compared to a distributed hydrological model, a lumped impulse response model is less time-consuming to construct and can be more effective to transform the input impulse to yield an accurate prediction of the

65 system output (Long, 2015; Olsthoorn, 2007; Asmuth and Knotters, 2004). The objectives are to (1) simulate the groundwater level in response to system input of precipitation and air temperature; (2) simulate the groundwater inflow to rivers in response to system input of groundwater level and compare the estimated groundwater inflow with the separated baseflow from different baseflow separation techniques; and (3) investigate the temporal variation, trend and seasonality of the meteorological and hydrological variables that characterize the lowland hydrological system. If this combined approach can be successfully

70 applied in these three specific catchments, it can potentially be applied to catchments with similar conditions worldwide.

2 Study area

The study focuses on three temperate lowland catchments in the northeastern and central Belgium: the Zwarte Beek, the Herk and Mombeek (main tributary of the Herk), and the Dijle catchments (Fig. 1). They are sub-catchments of the Scheldt river basin and cover an area of approximately 95, 272 and 893 km^2, respectively. The elevation ranges are 21–148 m TAW (Tweede

75 Algemene Waterpassing) for the Zwarte Beek, 25–133 m TAW for the Herk and Mombeek, and 9–177 m TAW for the Dijle. The highest point in the Zwarte Beek (148 m TAW) is the spoil tip of a coal mine. The climate of the area is humid temperate. The average annual precipitation is 824, 773 and 706 mm for the Zwarte Beek, the Herk and Mombeek, and the Dijle, respectively (KMI, 2020), observed between 1990 and 2019 from nearby meteorological stations (Fig. 1a). The average monthly precipitation data shows that August and December are the wettest months with 81 and 87 mm for the Zwarte Beek,

80 85 and 79 mm for the Herk and Mombeek, and 81 and 72 mm for the Dijle (Fig. 2). April is the driest month with 48, 45 and 39 mm of precipitation for the three catchments, respectively (Fig. 2). The average daily air temperature is approximately 11 °C for the three catchments during the same observation period (KMI, 2020). The hottest and coldest months are July and January with an average monthly air temperature around 19 and 4 °C, respectively (Fig. 2). The average annual potential open water evaporation varies between 662 and 675 mm, of which the summer (June–August) potential evaporation takes up

85 approximately 85 % of the total amount (Batelaan and De Smedt, 2007).
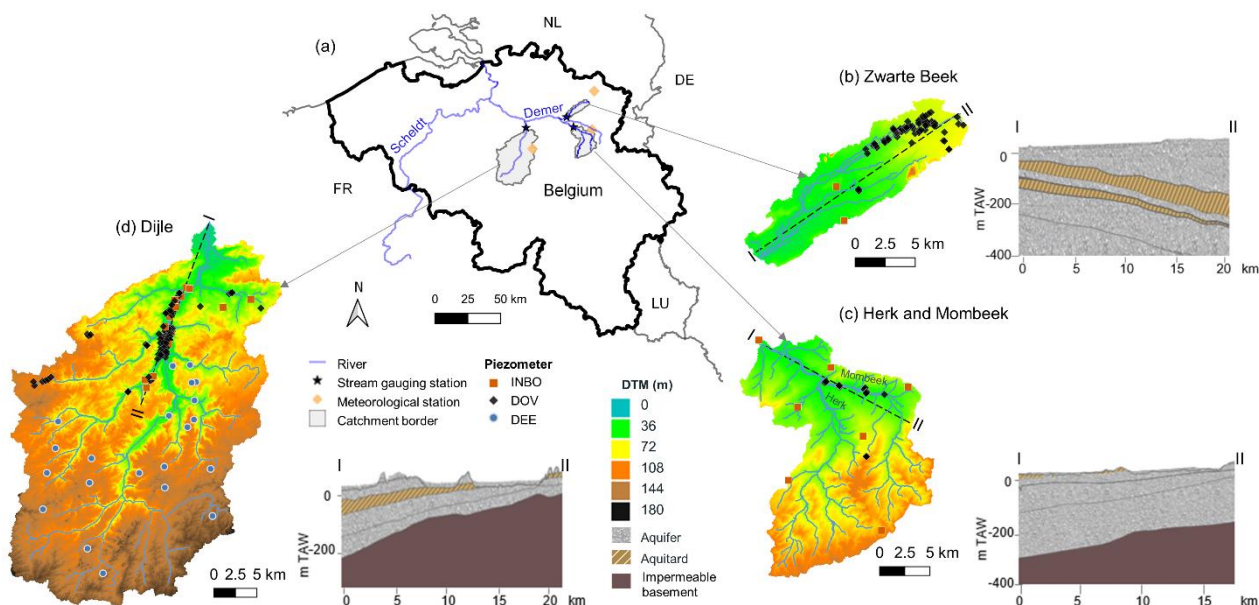
Figure 1 Location of the studied catchments in (a) the Scheldt river basin: (b) the Zwarte Beek, (c) the Herk and Mombeek, and (d) the Dijle; and the cross-sectional sketches of the hydrogeological layers (DOV, 2020) and piezometers in each catchment. DTM from Geopunt Vlaanderen (https://www.geopunt.be/).
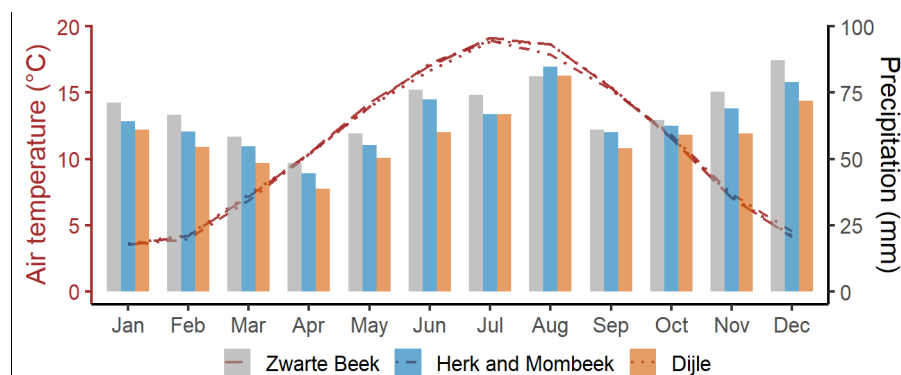
Figure 2 The average monthly precipitation and air temperature of the three catchments, based on daily observations between 1990 and 2019 (KMI 2020).

Both the Zwarte Beek and the Herk and Mombeek are tributaries of the Demer (Fig. 1a). The Demer joins the Dijle at Rotselaar, then heading towards the Scheldt estuary in Antwerp (Fig. 1a). The stream flows of the studied river segments are measured at the catchment outlet (Fig. 1a). The average daily stream flows are 1.05 m^3 s^{-1} for the Zwarte Beek, 1.44 m^3 s^{-1} for the Herk and Mombeek and 6.65 m^3 s^{-1} for the Dijle. The stream flow varies between 0.001–7.03 m^3 s^{-1} for the Zwarte Beek, 0.06–20.4

m³ s⁻¹ for the Herk and Mombeek, and 1.23–29.1 m³ s⁻¹ for the Dijle (Fig. 3a). The flow duration curve (FDC) plots the cumulative frequency of the stream flow and represents the variability of stream flow in a catchment (Vogel and Fennessey,

100   1994), with a flat slope indicating a groundwater-feeding surface storage and a steep slope revealing flashy flow regime dominated by direct runoff (Searcy, 1959). The flat slope of the FDCs (Fig. 3a) indicates that these perennial rivers have a strong groundwater feeding feature. The monthly average stream flows show that there is some seasonality in the time series, specifically, higher flows are observed during the winter months (December–February) than other seasons in all three catchments (Fig. 3b). For the Dijle catchment alone, the monthly average stream flows are relatively low in the spring (March–

105   May) and relatively high both in the summer and winter during the 30-year study period (Fig. 3b).
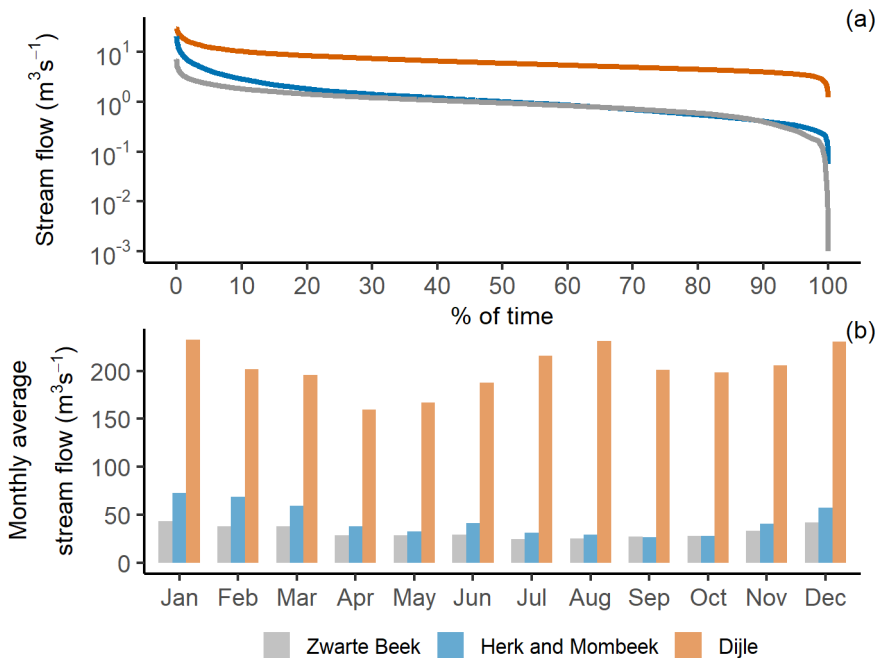
Figure 3 The FDC (a) and the average monthly stream flow (b) in the three catchments.

According to the Flanders subsurface database DOV (Databank Ondergrond Vlaanderen) and lithostratigraphic units, the

110   Zwarte Beek catchment mainly developed in sandy Neogene sediments, and the Boom and Kortrijk clay Formations (Fig. 1b) represent two aquitards (DOV, 2020; Laga et al., 2001). The surficial geology outside the floodplain is dominated by sand while the floodplain itself is dominated by sand and peat (DOV, 2020). The stream bed material varies from coarse sand upstream to fine sand downstream, as observed during field trips. The Herk and Mombeek catchment (Fig. 1c) developed mostly in sandy Palaeogene sediment with the Boom clay Formation at the shallow depth in the northern part (Laga et al.,

115   2001). The top of the impermeable basement consists of marl and clay from the Heers and Hannut Formations (DOV, 2020; Laga et al., 2001). The surficial geology outside the floodplain is dominated by loam and sandy loam while the floodplain itself is characterised by loam and clay sediments (DOV, 2020). The river bed of the Mombeek tributary consists mainly of

clay, as observed during field trips. The Dijle valley (Fig. 1d) mainly developed in Palaeogene and Neogene sands, but continued incision is the reason why the floodplain has reached the very impermeable clay from the Kortijk Formation below (DOV, 2020). The shallow geology outside the floodplain is dominated by loam and sandy loam deposits , and the floodplain itself consists of loam, sand, clay and peat (DOV, 2020).

The major land uses are crop (24.4 %), meadow (23.6 %) and urban area (15.2 %) for the Zwarte Beek catchment; meadow (56.0 %), orchard (21.1 %) and crop (11.3 %) for the Herk and Mombeek; and crop (35.6 %), meadow (28.1 %) and urban area (19.7 %) for the Dijle in 2012 (DOV, 2020). The urban coverage is relatively low in all three catchments. The upstream of the Zwarte Beek is within the military domain with little built-up area. There are several natural reserves within these catchments also. Since 1990, the Belgium government has carried out nature-based solutions for floodplain restoration and "zero management" polices to reduce the human impacts on catchments such as the Dijle (Turkelboom et al., 2021). Therefore, the three catchments are mostly under natural conditions during the study period.
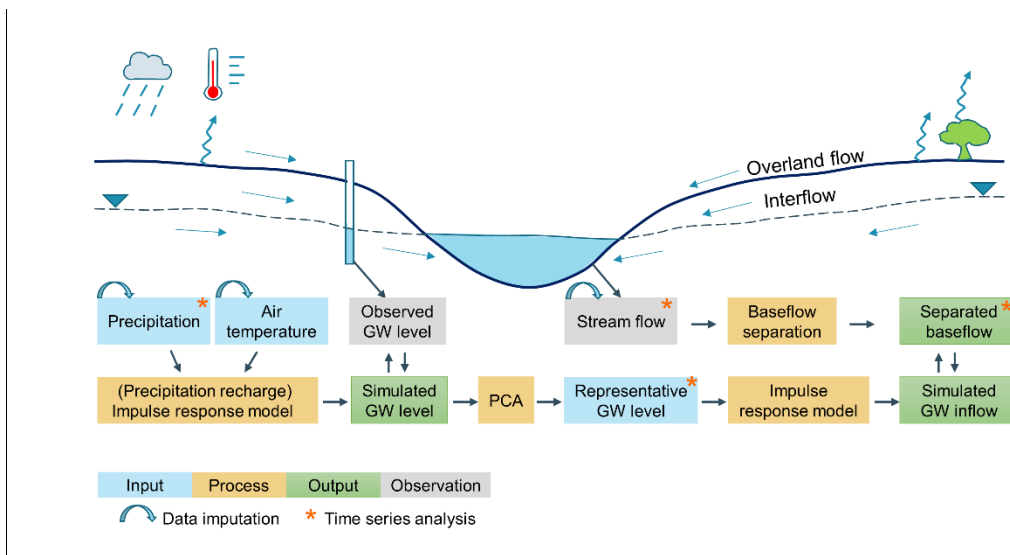
3 Methodology

Figure 4 An illustration of the methodology in this study. PCA is the abbreviation for principle component analysis.

An illustration of the methodology is shown in Fig. 4. First of all, precipitation, air temperature, groundwater level and stream flow data were collected and imputed where necessary. Afterwards, imputed precipitation and air temperature were used as system input for the first case in the impulse response model, and the system output was calibrated with observed groundwater level. Only well fitted groundwater level time series were retained and further used to generate a representative groundwater level time series via principle component analysis in each catchment. This time series was applied as system input for the

second case in the impulse response model. The model output of simulated groundwater inflow to rivers was calibrated with
140 separated baseflow obtained from hydrograph separation approaches. At last, time series analysis was carried out to investigate the temporal variation, trend and seasonality of the hydrological variables. Detailed explanations can be found in the following sections.

3.1 Data preparation

3.1.1 Data collection

145 The daily precipitation and daily air temperature were obtained from KMI (Koninklijk Meteorologisch Instituut) at the closest meteorological station for each catchment (Fig. 1a). The daily stream flow time series were accessed from https://www.waterinfo.be via the wateRinfo R package interface (Van Hoey, 2020) and from the river gauging station at the catchment outlet (Fig. 1a). These time series cover one climatic cycle of 30 years (1 Jan 1990–31 Dec 2019).

150 The groundwater levels were obtained from the piezometric observation network of INBO (Instituut voor Natuur- en Bosonderzoek), DOV and DEE (Département de l'Environnement et de l'Eau), respectively representing 82 %, 11 % and 7 % of the total number of 343 wells (Fig. 1b–d). The groundwater level time series from INBO are recorded daily. Mostly of the groundwater levels from the DOV are measured monthly, and the rest are recorded biweekly. The observations from the DEE are measured mostly on a weekly basis with the rest on a monthly basis.

155

In the Zwarte Beek and the Herk and Mombeek, the average groundwater depths to water table are 0.6 and 3.1 m, respectively, and the observations are all from shallow aquifers, with the groundwater depth to water table less than 17.8 m. In the northern Flemish part of the Dijle catchment, the groundwater level time series are located in the very shallow part of the aquifer, with an average depth to the water table of 1.1 m. In the southern Walloon region of the Dijle catchment, where the elevation
160 differences are larger than in the north, we obtained a very limited number of observations (23) from DEE (Fig. 1d) and included them all to avoid data absence in that region. The groundwater depth to water table there has a mean value of 25.3 m. The time spans of the groundwater level observations vary between 2 and 30 years, with an average of 16.2 years. The time series which covered short periods (e.g. a few months) or were very discontinuous were excluded. With the monthly frequency, time series consisting of at least 90 data points were considered to be adequate, which corresponded to one fourth (7.5 years)
165 of the full time period.

3.1.2 Data imputation

The missing values in the raw time series were imputed, as required for further analysis. The imputation techniques applied in this study were (1) linear or local polynomial regression models for estimations based on different time series and (2) ordered quantile normalization for re-scaling different time series (Fan and Gijbels, 2018; Peterson and Cavanaugh, 2019). A time

series of a nearby station that survived the quality checks and has less missing values, is used as the reference series to check first if a linear regression model would be adequate ($R^2 \geq 0.7$). If not satisfactory, a local polynomial regression model is applied instead. When the linear regression model is not adequate, another option is to perform the ordered quantile normalization. The marginal distribution of the target series is in this case approximated, using days with observations in both series, by transforming both with ordered quantile normalization and making the two distributions identical in statistical properties (Peterson and Peterson, 2020).

3.2 Baseflow separation

Baseflow separation divides the stream flow into the components that originate (1) from quick flow, the sum of water derived from precipitation which contributes to the stream soon after rainfall events, and (2) baseflow, from groundwater discharge or other delayed sources (Hall, 1968; Nathan and McMahon, 1990; Piggott et al. 2005). The main separation techniques include (1) the graphic methods, which pick out the low-flow points from the hydrographs and link them together as the baseflow component (Sloto and Crouse, 1996; Rutledge, 1998), and (2) the digital filter methods, which filter out a low frequency signal representing baseflow and a high frequency signal attributed to the quick flow (Nathan and McMahon, 1990; Arnold and Allen, 1999; Eckhardt, 2005, 2008; Jakeman and Hornberger, 1993). The base flow index (BFI) gives the ratio of the baseflow to the total stream flow. It is an indicator of the catchment flow regime, with high indices (>0.9) for permeable catchments with a very stable flow regime and low indices (0.15–0.2) for impermeable catchments with a flashy flow regime (Tallaksen and Van Lanen, 2004). Although it is difficult to validate the separated baseflow and there is lack of presentation of the physical processes of the river–aquifer exchange (Sloto and Crouse, 1996; Batelaan and De Smedt, 2007; Killian et al., 2019), baseflow separation is still a fast, efficient, and widely used approach to quantitatively estimate the baseflow at the catchment scale.

In this study, we used different baseflow separation methods to provide an idea on the range of potential outcomes. The selected approaches were (1) graphical separation techniques from HYSEP (Sloto and Crouse, 1996), including fixed interval, sliding interval and local minimum technique; (2) one-parameter digital filter method from Nathan and McMahon (1990), where the filter parameter is taken as 0.925; and (3) two-parameter digital filter method from Eckhardt (2005, 2008), since this method agrees well with tracer based (e.g. dissolved silica) hydrograph separation in lowland catchments (Gonzales et al., 2009). The filter parameter is set as 0.98 and the BFI_{max} parameter is chosen as 0.80 for the Eckhardt method, recommended by other research conducted with the same method in Flanders (Zomlot et al., 2015).

3.3 Impulse response modelling

3.3.1 Model overview

A lumped parameter impulse response model can effectively transform a hydrological system input to yield an accurate prediction of the corresponding system output, and the impulse response function (IRF) estimated in the model can provide

mechanistic insights into the hydrological system, such as the peak response time and magnitude (Olsthoorn, 2007; Asmuth and Knotters, 2004; Young, 2013). The impulse response model used in this study is the Rainfall-Response Aquifer and Watershed Flow Model (RRAWFLOW; Long,2015). RRAWFLOW includes two processes, (1) the process of recharge generation from precipitation, denoted as precipitation recharge in this study, and (2) the process of precipitation recharge transitioning into a system response such as groundwater level or spring flow (Long and Mahler, 2013; Long, 2015).

During the first nonlinear process, the precipitation recharge is estimated by using a unitless soil–moisture index s (Long and Mahler, 2013). This s (≤ 1.0) represents the fraction of precipitation that infiltrates and becomes precipitation recharge. Since the preceding rainfall events have impacts on soil moisture, the past rainfall record is counted and weighted by an exponential decay function (Jakeman and Hornberger, 1993). Detailed equations and parameterization can be found in Long and Mahler (2013).

During the second process, the response of the hydrological system to the precipitation recharge is estimated by convolution (Long, 2015), which is the superposition of a series of IRFs that are initiated at the time of each impulse and scaled proportionally by the magnitude of the corresponding impulse (Olsthoorn, 2007; Long and Mahler, 2013; Asmuth et al., 2002). The discrete form of the convolution integral for uniform time steps used in RRAWFLOW is:

$$y_i = \Delta t \sum_{j=0}^{i} \beta_j h_{i-j} u_j + \psi_i + d_0 \tag{1}$$
$$i, j = 0, 1, \ldots, N$$

where h_{i-j} is the IRF; u_j is the input; j and i are time step indices corresponding to system input and output, respectively; Δt (T) is the time step duration; N (unitless) is the number of time steps in the output record; β_j (unitless) is an optional scaling coefficient of IRF; ψ_i is the error component resulting from inaccuracy in measurement, sampling intervals, or model simplification assumptions; and d_0 is a hydraulic-head datum (L) for groundwater level simulation (Long, 2015). In this process, precipitation recharge (u_j) is assumed to be the only forcing that can cause an increase in the hydraulic head to be above d_0 (Long, 2015).

Hydrological system dynamics can be approached by different types of parametric IRFs. In this study, we use parametric gamma functions, as they tend to work well and allow us to easily evaluate the fitted parameters. The gamma function and gamma distribution function in RRAWFLOW are:

$$\Gamma(\eta) = \sum_{t=0}^{\infty} t^{\eta-1} e^{-t} dt \tag{2}$$

$$\gamma(t) = \frac{\lambda^{\eta} t^{\eta-1} e^{-\eta t}}{\Gamma(\eta)} \tag{3}$$

$$h(t) = \epsilon \gamma(t) \tag{4}$$

where Γ and γ are gamma function and gamma distribution function, respectively; λ (unitless) and η (unitless) are shape parameters; t (T) is the time centred on each discrete time step; h is the scaled gamma distribution function; and ϵ (unitless)

is the scaling coefficient that compensates for the system response when there is not a one–to–one relation between system input and output (Olsthoorn, 2007; Long, 2015). RRAWFLOW allows the use of two superposed gamma distribution functions, which represent the components of quick flow and slow flow in the hydrological system, and it also allows the system records to be divided into two periods, namely dry and wet periods (Long, 2015).

The "L-BFGS-B" method is used for RRAWFLOW optimization, which allows working with lower and upper parameter bounds (Byrd et al., 1995). The Nash–Sutcliffe Efficiency (NSE) is used for the evaluation of the simulated time series (Nash and Sutcliffe, 1970). NSE = 1 means a perfect model fit, and NSE = 0 indicates that the model has the same predictive power as the mean of the time series in terms of the sum of the squared error, and if NSE < 0, it is worse than the observed mean (Nash and Sutcliffe, 1970).

We use RRAWFLOW to explore the hydrological system response of groundwater level to meteorological forcing (Sect. 3.3.2) and groundwater inflow response to groundwater level as system input (Sect. 3.3.3), under natural conditions. The model parametrization and modifications to the original RRAWFLOW code are discussed below.

3.3.2 Groundwater level response modelling

The groundwater level response modelling consists of precipitation recharge generation and recharge transitioning into groundwater level. The system input is precipitation and air temperature data, and the system output is compared with groundwater level observations. The model time–step interval is daily, which is determined by the input time series of precipitation and air temperature. A warm-up period of six years was added (1984–1989), using the data record from the first six years (1990–1995). This estimated warm–up period can largely reduce the antecedent effects of the system before it is fully incorporated into the simulation.

To better represent the transient characteristics of the hydrological system, the dry (April–September) and wet (October–March) periods were defined, because of very different evapotranspiration effects within the year (Fig. 2). Different gamma distribution functions are used for representing quick and slow components as well. In total, four gamma distribution functions are used in the simulation, representing the quick flow and slow flow processes during both the dry and wet periods. In each gamma distribution function, there are three parameters to be optimized, two shape parameters (λ and η, Eq. 3) and one scaling coefficient (ϵ, Eq. 4). The double–gamma IRFs representing dry (h_{dry}) and wet (h_{wet}) periods are shown below:

$$h_{dry}(t) = \epsilon_1 \frac{\lambda_1^{\eta_1} t^{\eta_1-1} e^{-\eta_1 t}}{\Gamma(\eta_1)} + \epsilon_2 \frac{\lambda_2^{\eta_2} t^{\eta_2-1} e^{-\eta_2 t}}{\Gamma(\eta_2)} \tag{5}$$

$$h_{wet}(t) = \epsilon_3 \frac{\lambda_3^{\eta_3} t^{\eta_3-1} e^{-\eta_3 t}}{\Gamma(\eta_3)} + \epsilon_4 \frac{\lambda_4^{\eta_4} t^{\eta_4-1} e^{-\eta_4 t}}{\Gamma(\eta_4)} \tag{6}$$

where the subscripted number 1 and 2 for quick and slow components during dry period, and 3 and 4 for quick and slow components during the wet period. Besides the 12 parameters from the IRFs (Eq. 5–6), the hydraulic-head datum parameter (d_0, Eq. 1) is also included for optimization.

Although the IRFs can have infinite length, we define the system has a maximum memory of six years for an impulse, to avoid long–term trends or human interference effects to bias the fitted IRFs. The whole 30–year period is used for model calibration, as we are doing exploratory rather than confirmatory analysis here.

3.3.3 Groundwater inflow response modelling

The groundwater inflow response modelling simulates the process of groundwater discharge to rivers. Fitted groundwater levels from the previous step are used for this process. As there are many groundwater level time series in each catchment, we introduce a single representative groundwater level time series, to reduce the dimensionality of the problem. The representative groundwater level time series was obtained by extracting the first principle component of the fitted groundwater level time series, to represent the catchment status in terms of groundwater level.

The model was set up with the representative groundwater level as the system impulse and separated baseflow as the system response. A six–year warm–up period (1984-1989) was again added, using the representative groundwater level time series for the period between 1990 and 1995. As the groundwater discharge to stream flow happens beneath the land surface, without the pronounced wet–dry period distinctions from the effects of evapotranspiration, a time–invariant model is assumed for this modelling process. Only two gamma distribution functions are thus used, for representing the quick and slow components. The compound IRF (h_{comp}) is shown below:

$$h_{comp}(t) = \epsilon_q \frac{\lambda_q^{\eta_q} t^{\eta_q - 1} e^{-\eta_q t}}{\Gamma(\eta_q)} + \epsilon_s \frac{\lambda_s^{\eta_s} t^{\eta_s - 1} e^{-\eta_s t}}{\Gamma(\eta_s)} \tag{7}$$

where the subscripted letter q and s for quick and slow components, respectively.

Furthermore, a modification is made to the original code, where a constant drainage level is subtracted from the input groundwater level. This operation turns the representative groundwater level into a proxy for the hydraulic gradient. The modified convolution integral has the form as below:

$$y_i^{mod} = \Delta t \sum_{j=0}^{i} \beta_j \, h_{i-j}(u_j - d_0) + \psi_i \tag{8}$$

There are hence seven parameters to be optimized: three parameters (λ, η and ϵ) for each of the two gamma distribution functions and the drainage level, which was actually implemented by using the hydraulic-head datum d_0. This allowed the modification to be made with minimal code adjustments.

3.4 Time series analysis

295 Hydrological time series usually have strong seasonal variations and can be decomposed using an additive approach to study the temporal evolution of the different components. In this study, we apply the Seasonal and Trend decomposition with Loess (STL) to decompose the time series into three components: (1) a trend-cycle component, (2) a seasonal component, and (3) a reminder component (Cleveland et al., 1990). The additive decomposition of the target time series has the following form:

$$y_t = T_t + S_t + R_t \qquad (9)$$

300 where y_t is the seasonal time series; T_t is the smoothed trend-cycle component; S_t is the seasonal component; and R_t is the remainder component (Cleveland et al., 1990).

The features of the STL decomposition are summarized using two parameters:

   1. the strength of the trend:

305
$$F_t = max(0, 1 - \frac{Var(R_t)}{Var(T_t + R_t)}) \qquad (10)$$

with F_t close to zero, representing a weak trend, and closer to one, representing a strong trend, and

   2. the strength of the seasonality:

$$F_s = max(0, 1 - \frac{Var(R_t)}{Var(S_t + R_t)}) \qquad (11)$$

with F_s close to zero indicates a weak seasonality, and close to one indicates a strong seasonality (Hyndman and

310 Athanasopoulos, 2021).

The decomposed hydrological variables include precipitation, representative groundwater level, stream flow and separated baseflow. The trend analysis uses a window of 365 consecutive daily observations for estimating the trend–cycle component on a yearly basis. This span allows the retention of sufficient fluctuation in the data. The seasonal component analysis takes

315 365 days as its periodic cycle and a window of 11 consecutive years for estimating the seasonality.

4 Results

4.1 Separated baseflow

Figures 5 to 7 show the temporal evolution of the separated baseflow on a daily basis and the comparison of the stream flow and baseflow by different methods in the three catchments. The fixed interval and sliding interval approaches yield slightly

320 higher estimated mean BFIs than other methods, since they capture quite a large amount of baseflow from the peak flows and high flow periods in the stream flow record (Fig. 5a–b; Fig. 6a–b; Fig. 7a–b). The local minimum and Eckhardt methods result in slightly lower mean BFIs than the previous two methods, as they tend to filter out large impact of high stream flow events on the baseflow (Fig. 5c–d; Fig. 6c–d; Fig. 7c–d). The estimated mean BFI from the Nathan approach is the lowest among all

the methods, and the separated baseflow time series has less amplitude variation over time and is less influenced by high stream

325   flows than the other methods (Fig. 5e; Fig. 6e; Fig. 7e). The mean BFIs over the 30–year period range between 0.73–0.86 for

the Zwarte Beek, 0.70–0.82 for the Herk and Mombeek and 0.77–0.84 for the Dijle.
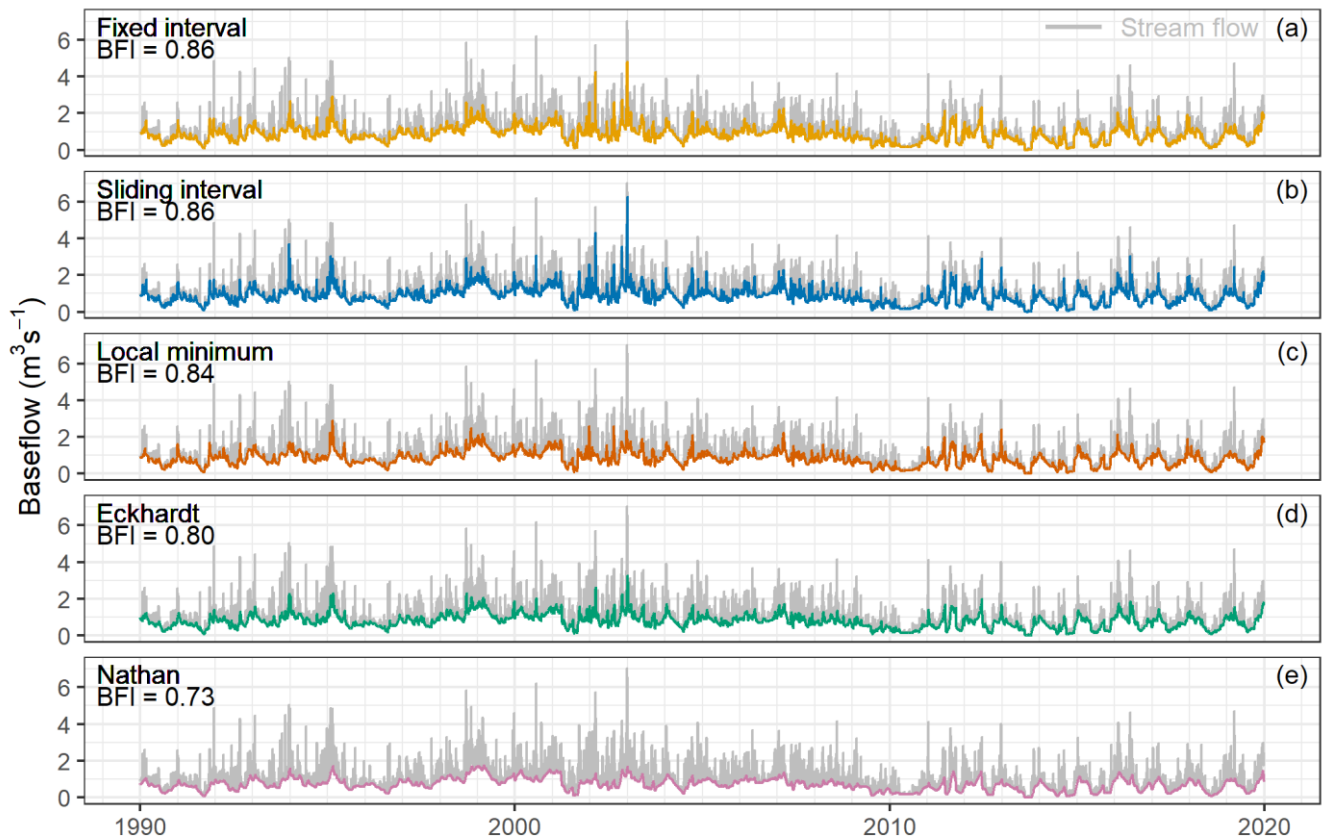
330   **Figure 5** The separated baseflow and stream flow time series over the 30–year study period in the Zwarte Beek.
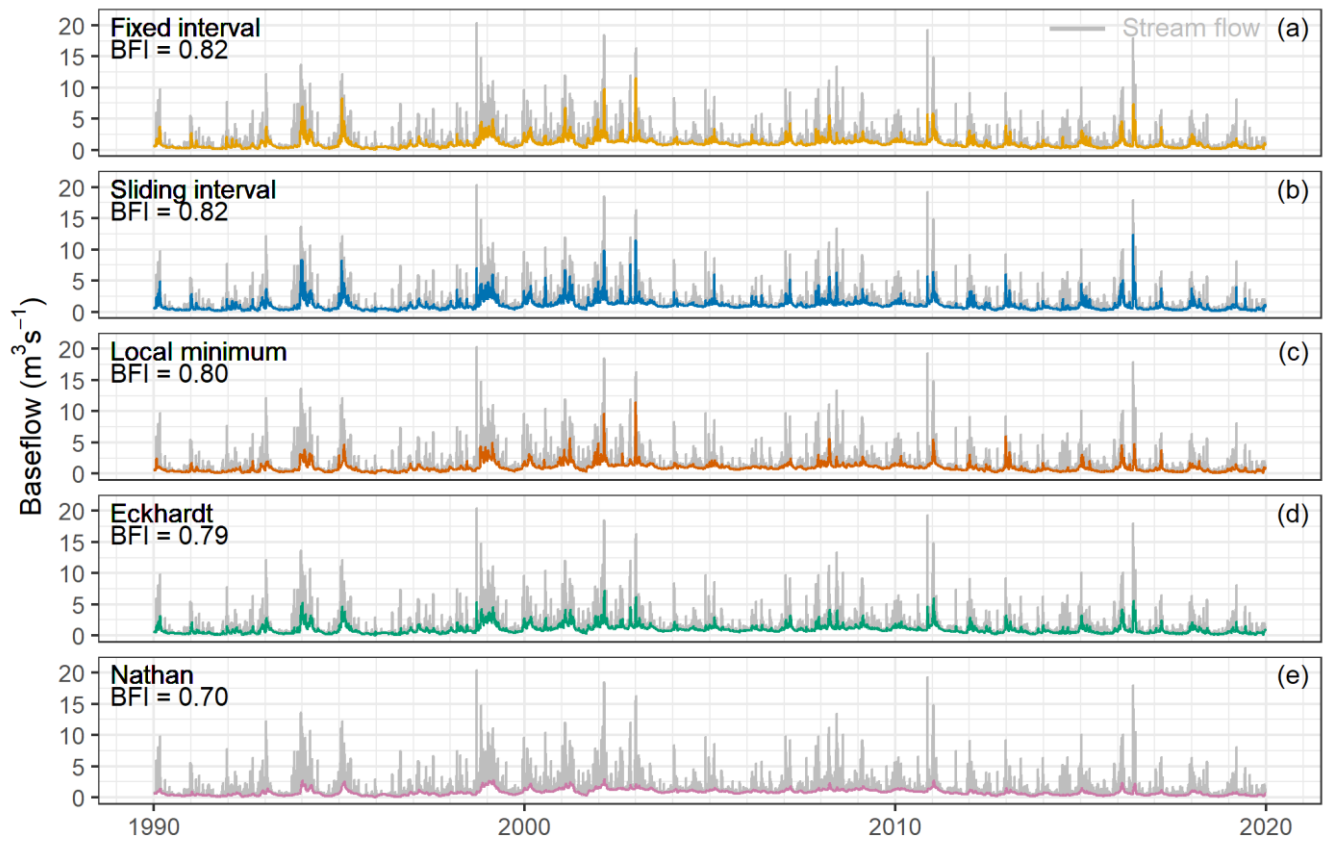
Figure 6 The separated baseflow and stream flow time series over the 30–year study period in the Herk and Mombeek.

335
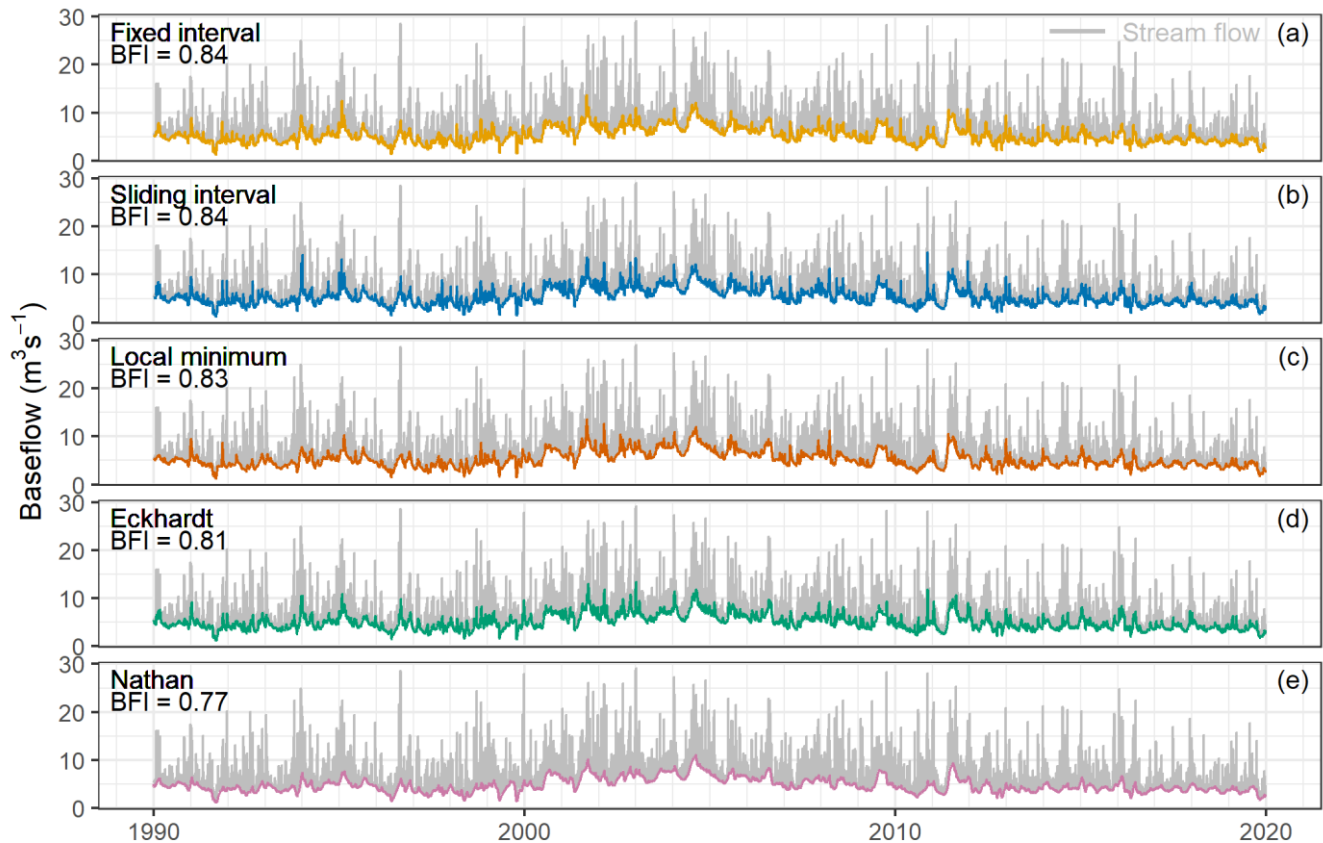
Figure 7 The separated baseflow and stream flow time series over the 30–year study period in the Dijle.

4.2 Impulse response modelling of the hydrological system

4.2.1 Groundwater level response modelling

Altogether, 100 groundwater level time series in the Zwarte Beek, 45 in the Herk and Mombeek and 198 in the Dijle were used for the groundwater level response modelling. The positive NSEs (0–1) of the simulated time series take up 89 %, 95 % and 83 % of all the simulations in the Zwarte Beek, the Herk and Mombeek and the Dijle, respectively. The overall model performance is better in the Zwarte Beek and the Herk and Mombeek than the Dijle. Taking into account the balance between evaluating model performance and allowing sufficient simulated time series to compute the representative groundwater level, we considered the simulations with a NSE > 0.3 as satisfactory. This allowed 70 simulated time series for the Zwarte Beek, 38 for the Herk and Mombeek and 108 for the Dijle to be retained. Examples of the retained groundwater level time series for each catchment are shown in Fig. 8. The time series for the Zwarte Beek and the Herk and Mombeek (Fig. 8a–b) seem to be reproduced by the impulse response model in a very detailed way (NSEs > 0.8), while the time series for the Dijle (Fig. 8c)

350 seems to exhibit very low levels in the middle or second half of the year, and apparently is not straightforward to be captured with the impulse response modelling.
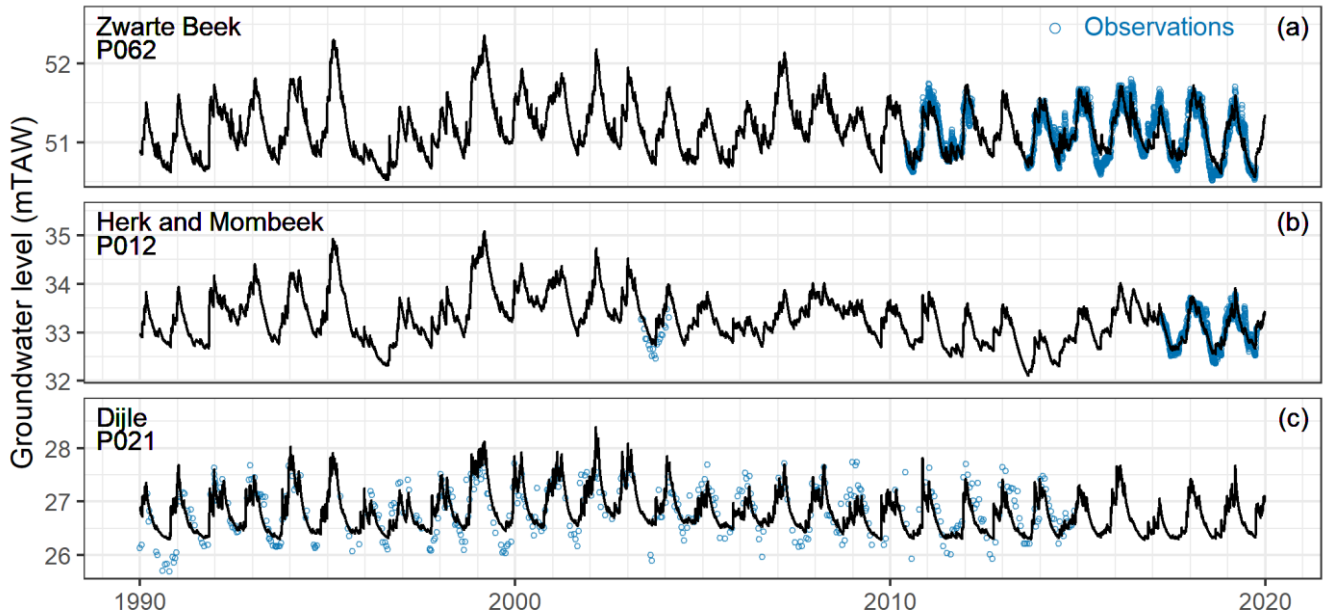
Figure 8 Selected observed and simulated groundwater level time series for impulse response modelling: (a) ZWAP062 in the
355 Zwarte Beek (NSE = 0.838), (b) MOMP012 in the Herk and Mombeek (NSE = 0.857) and (c) DYLP021 in the Dijle (NSE = 0.583).

The IRF curves from the modelling are shown in Fig. 9 for each retained groundwater level time series in the three catchments. Based on these IRFs, we extracted the peak time, representing the time it takes for the groundwater level response to reach its
360 maximum value due töo precipitation recharge, and the corresponding peak response (Fig. 10).
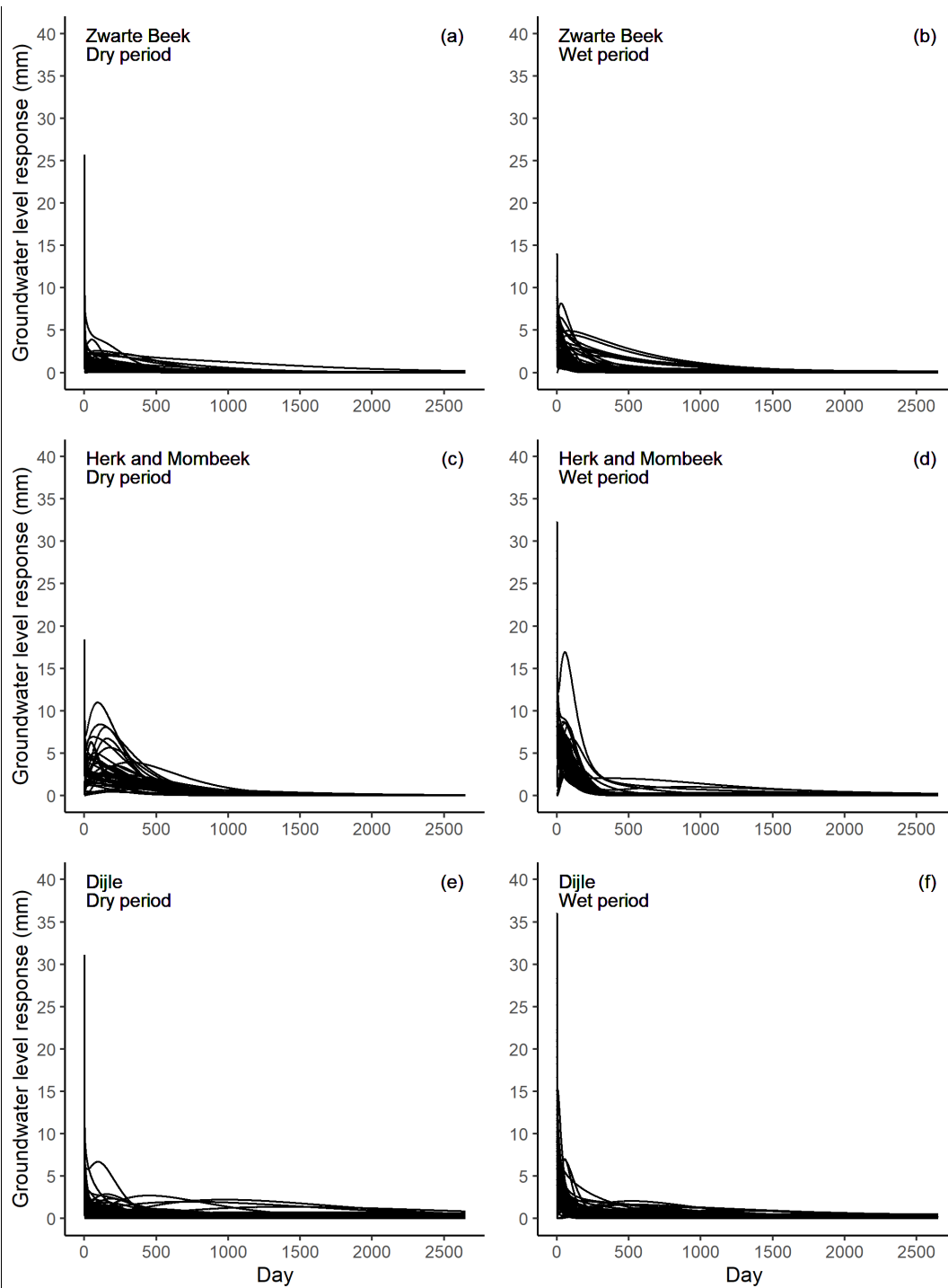
Figure 9 IRFs derived from the groundwater level response modelling for dry (April–September) and wet (October–March) periods in the three catchments.
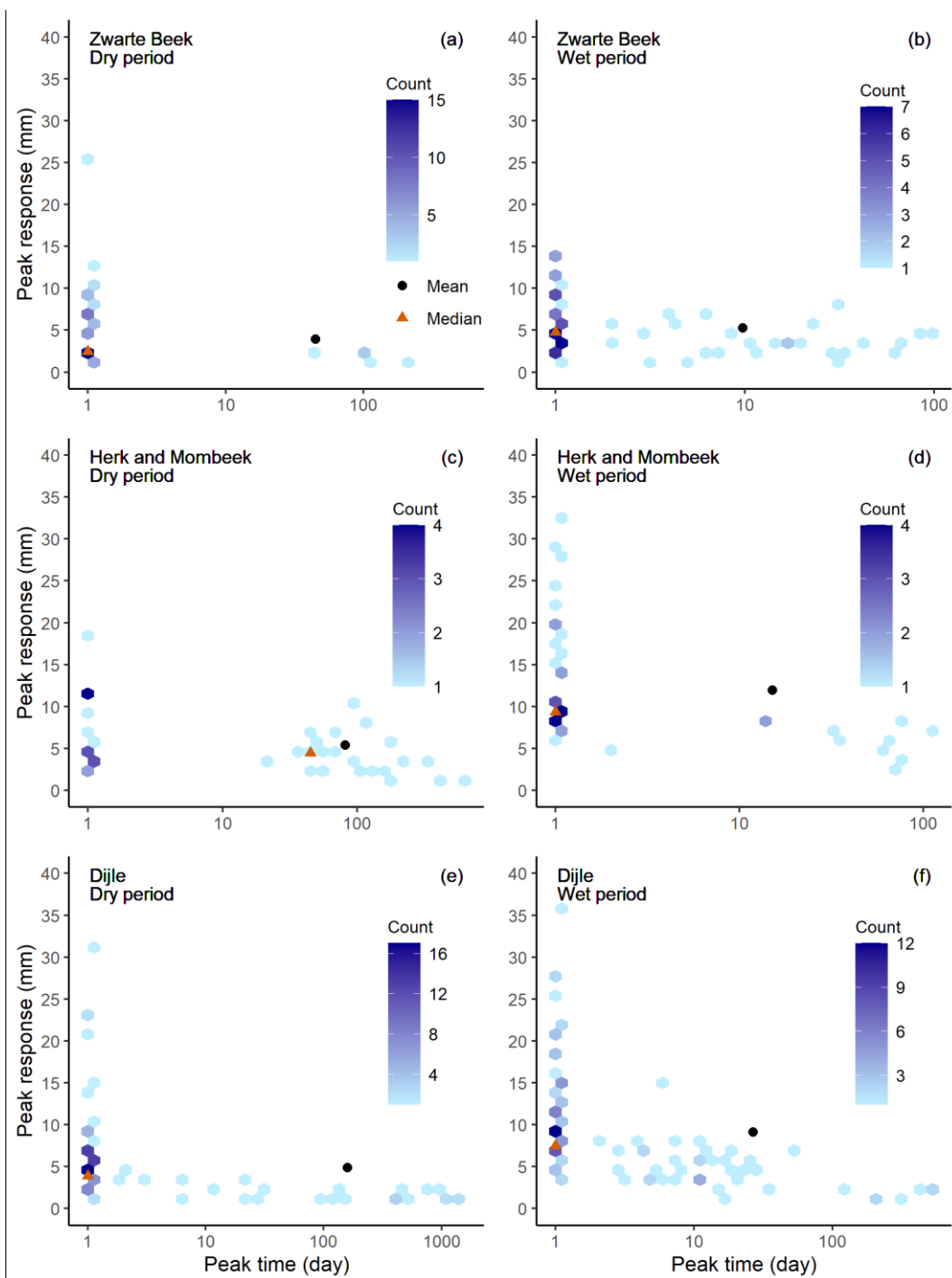
365 **Figure 10** Peak time and peak groundwater level response derived from the groundwater level response modelling for dry (April–September) and wet (October–March) periods in the three catchments.

In the Zwarte Beek, approximately 73 % (51/70) of the retained groundwater level wells in the dry period (April–September) and 61 % (43/70) in the wet period (October–March) reach its peak response in the first day (Fig. 9a–b; Fig. 10a–b). This indicates a very fast response to precipitation recharge in the shallow aquifer. The rest of the level time series has the peak time ranging between 2 and 548 days during the dry period (Fig. 10a) and between 2 and 98 days during the wet period (Fig. 10b). On average, it takes 45 days in the dry (Fig. 10a) and 10 days in the wet period (Fig. 10b) for the shallow aquifer to obtain its maximal response to precipitation recharge. For the response magnitude, 1 mm of precipitation recharge can cause a maximal immediate groundwater level rise between 0.01 and 25.7 mm during the dry period (Fig. 10a), and between 0.8 and 14.0 mm during the wet period (Fig. 10b). The mean peak responses are 3.9 and 5.3 mm for the dry and wet seasons, respectively (Fig. 10a–b). Relatively higher immediate increase of groundwater level occurs in the wet than the dry period.

In the Herk and Mombeek, around 42 % (16/38) of the groundwater level time series in the dry period and 71 % (27/38) in the wet period reach their peak response in the first day (Fig. 9c–d; Fig. 10c–d). For the rest, the range of the peak time is larger in the dry period (2–570 days; Fig. 10c) than the wet period (2–104 days; Fig. 10d). The mean peak time is 81 and 15 days for the dry and wet periods, respectively (Fig. 10c–d). Therefore, there is a clear trend of much faster response of the shallow aquifer to precipitation recharge in the wet period than the dry period. Regarding the peak response magnitude, the range is between 0.8 and 18.4 mm for 1 mm of precipitation recharge in the dry period (Fig. 10c), and between 2.6 and 32.3 mm in the wet period (Fig. 10d). The mean peak magnitudes are 5.4 and 12.0 mm for dry and wet periods, respectively (Fig. 10c–d). There is a general spatial trend observed in this catchment. If an observation well is closer to the river or the groundwater depth to water table is smaller, the peak time is relatively shorter and the peak response is higher.

During the dry period in the Dijle, approximately 68 % (73/108) of the observation wells reach their peak response in the first day while the remaining ones vary between 2 and 574 days (Fig. 9e; Fig. 10e). During the wet period, around 59 % (64/108) reach their peak response in the first day, and the rest peaks between 2 and 528 days (Fig. 9f; Fig. 10f). The mean peak time is 159 and 27 days for the dry and wet periods, respectively (Fig. 10e–f). The peak response ranges between 0.02 and 31.1 mm for the dry period (Fig. 10e), and between 0.6 and 36.1 mm for the wet period (Fig. 10f) for 1 mm of precipitation recharge. The mean peak response magnitudes are 4.9 and 9.2 mm for the dry and wet periods, respectively (Fig. 10e–f).

4.2.2 Groundwater inflow response modelling

The retained groundwater level time series from the previous simulations are used to generate a time series of the groundwater level for representing groundwater storage over the entire catchment. The extracted first principle component of the simulated groundwater levels takes up 83 %, 91 % and 79 % of the total variance, for the Zwarte Beek, the Herk and Mombeek, and the Dijle, respectively (Fig. 11b, d, f). The representative groundwater level time series has a mean of zero and the level is rescaled to a relative elevation (in meter, dividing the scores of the first principle component by the sum of the loadings) since only the level differences are relevant for the groundwater inflow response modelling (Fig. 11a, c, e). This time series can be interpreted

 intuitively as the relative difference of the groundwater level across the catchment at a certain point-in-time, with the average groundwater level.
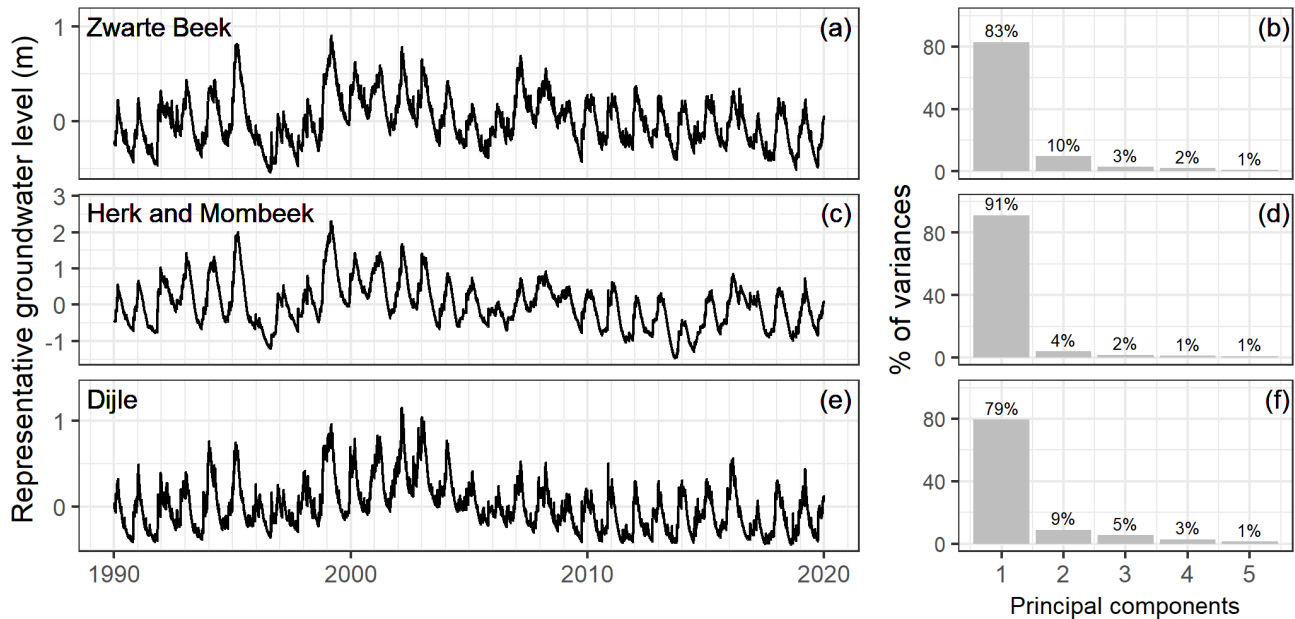
Figure 11 The representative groundwater level (relative elevation) time series and the variance proportions of the first five 405 principle components in each catchment.

The mean NSEs of simulated baseflow time series are 0.325 for the Zwarte Beek, 0.384 for the Herk and Mombeek and 0.146 for the Dijle. The Eckhardt and Nathan methods work better than other methods in the Zwarte Beek, with a NSE of 0.385 and 0.377, respectively. The Nathan method yields a higher NSE of 0.478 than other methods in the Herk and Mombeek. In the 410 Dijle, the Eckhardt method performs better than other methods with a NSE of 0.212. The IRFs extracted from the modelling show that there is basically an immediate response in the first time step, and the responses for a few days are already negligible. This means that our impulse response model basically falls back to a linear regression model of the groundwater inflow in function of the representative groundwater level, where the intercept and the slope are related to the drainage level and impulse response function value for the first time step, as shown in Table 1. The mean peak response, calculated as the mean value of 415 the slopes in Table 1, shows an average change of 0.95 m^3 s^{-1} of baseflow in the Zwarte Beek, 0.69 m^3 s^{-1} in the Herk and Mombeek and 2.2 m^3 s^{-1} in the Dijle, as a response of 1 m change in the groundwater level.

Table 1 The linear regression fit of the groundwater inflow as a function of the representative groundwater level in each catchment. Level = representative groundwater level; Fixed interval, Sliding interval, Local minimum, Eckhardt and Nathan 420 refer to different separation techniques.

Catchment	Fixed interval–Level	Sliding interval–Level	Local minimum–Level	Eckhardt–Level	Nathan–level
Zwarte Beek	y = 1.03 x + 0.92	y = 1.04 x + 0.92	y = 0.98 x + 0.89	y = 0.92 x + 0.79	y = 0.8 x + 0.71
Herk and Mombeek	y = 0.75 x + 1.02	y = 0.76 x + 1.02	y = 0.69 x + 0.97	y = 0.74 x + 0.98	y = 0.52 x + 0.81
Dijle	y = 2.16 x + 5.3	y = 2.26 x + 5.3	y = 2.07 x + 5.22	y = 2.65 x + 5.08	y = 1.88 x + 4.83

The simulated time series of groundwater inflow to the river tend to be smoother than the separated baseflow time series (Fig. 12–14). For the Zwarte Beek, the simulated groundwater inflow in the first two decades (1990–2009) can capture most of the low points, while for the last decade (2010–2019), there are some continuous periods with overestimation (Fig. 12). In the Herk and Mombeek, the simulated groundwater inflow time series seem to match well with the separated baseflow between 2005 and 2010 and major model overestimation occurs in the first decade (Fig. 13). For the Dijle, the differences between the simulated groundwater inflow and separated baseflow are relatively larger than the other catchments. For periods with decreased or increased fluctuations in separated baseflow (e.g. 1996–1999, 2000–2008), the groundwater inflow varies less intense (Fig. 14).

430
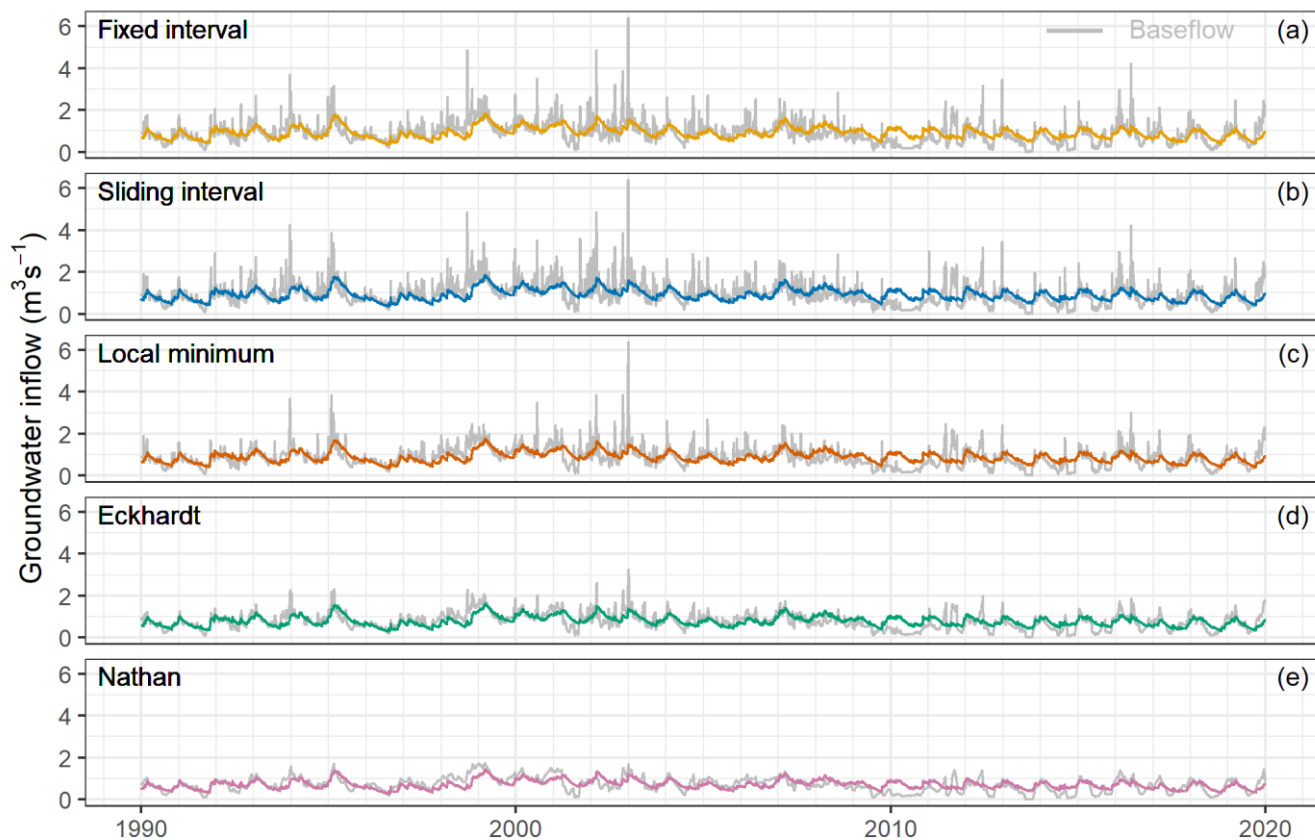
Figure 12 The comparison between the simulated groundwater inflow and the separated baseflow in the Zwarte Beek.
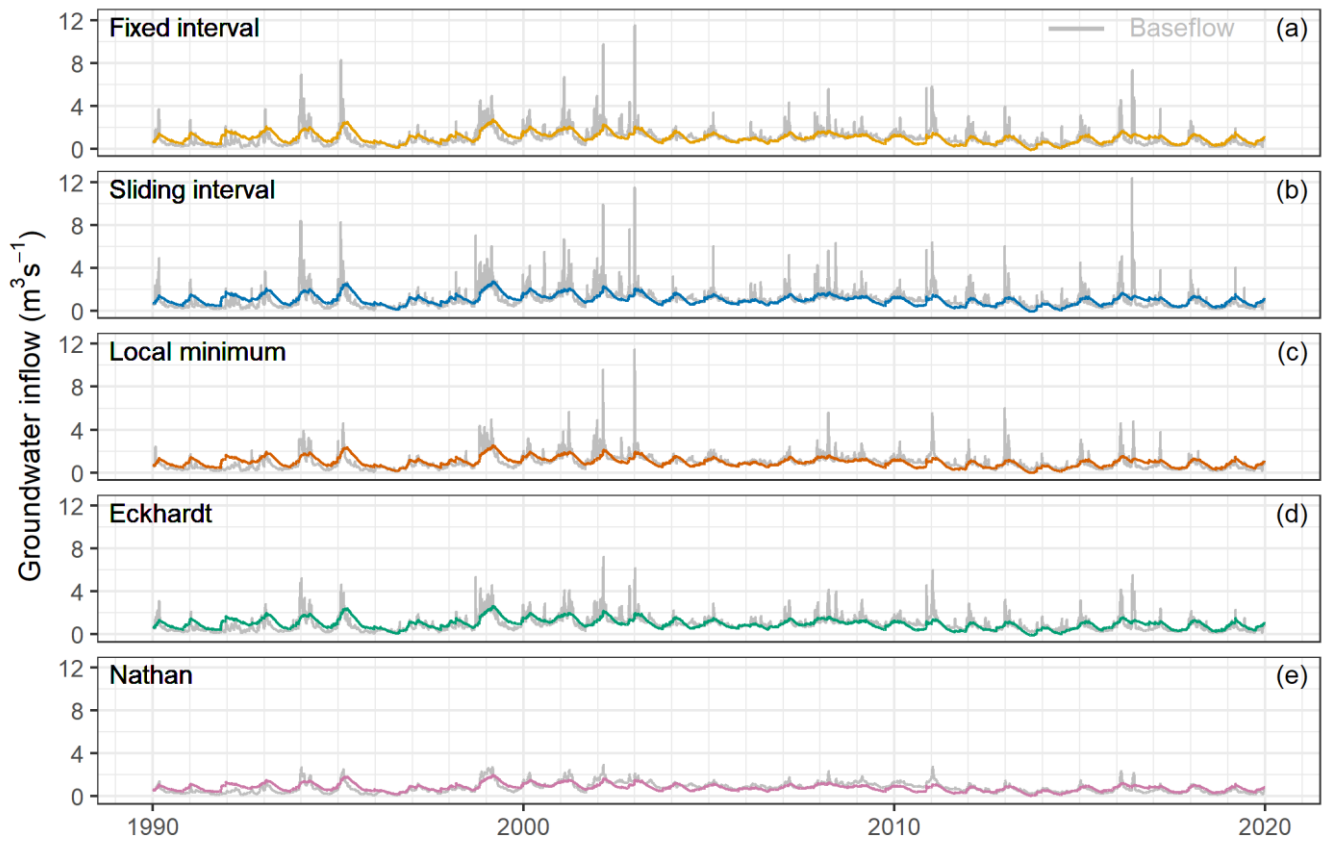
435

Figure 13 The comparison between the simulated groundwater inflow and the separated baseflow in the Herk and Mombeek.
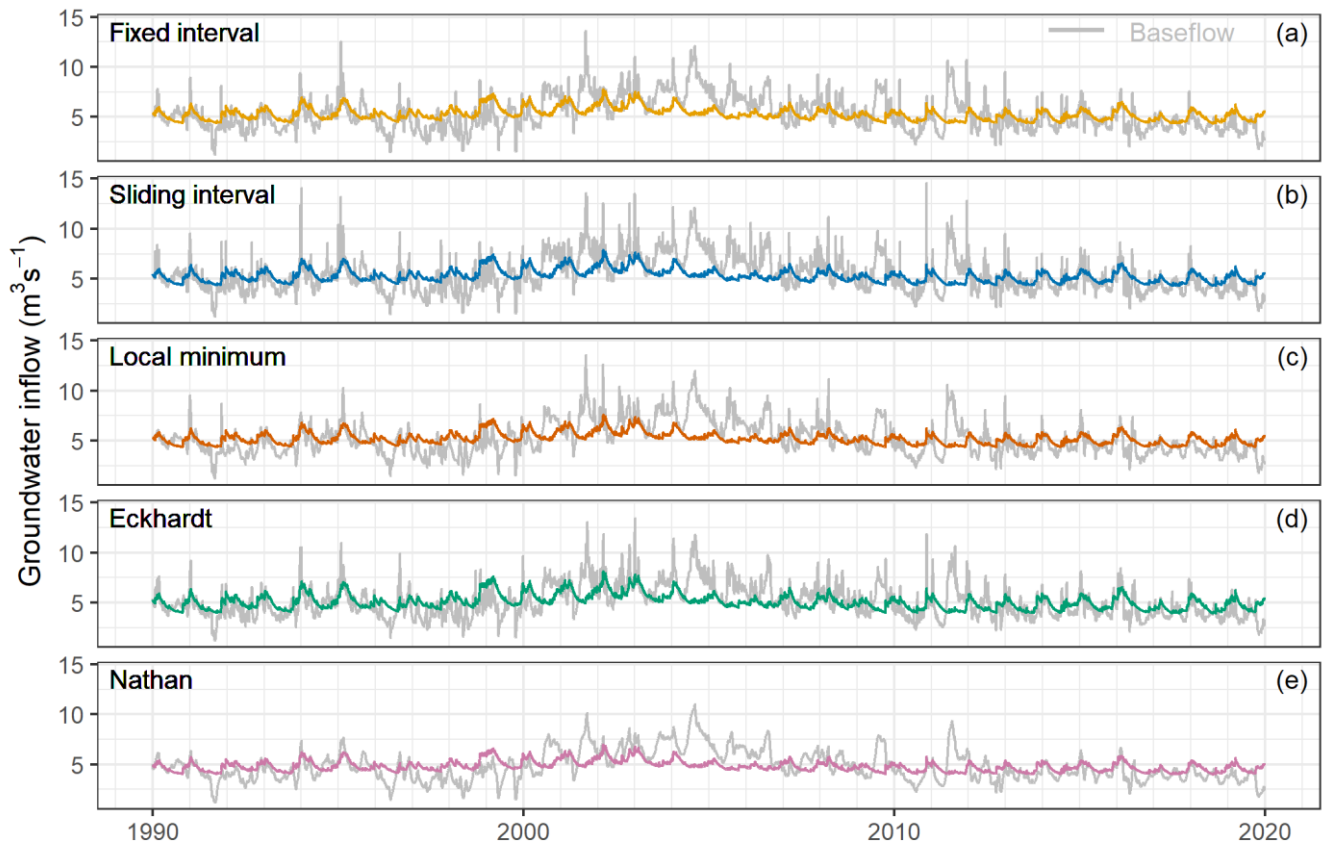
 Figure 14 The comparison between the simulated groundwater inflow and the separated baseflow in the Dijle.

4.3 Time series analysis

Precipitation has little trend over the 30–year period and the magnitudes of the extracted trend components are much smaller than the raw time series (Fig. 15a; Fig. 16a; Fig. 17a; Fig. 18). There is some level of seasonality observed for the precipitation, and the amplitudes of the seasonal components vary a lot between different years (Fig. 15b; Fig. 16b; Fig. 17b; Fig. 18). The
445 representative (Rep.) groundwater level time series has strong trend and seasonal strengths, and locates in the cluster formed by the individual (Indiv.) groundwater level time series, which indicates that it is a good representation of the catchment status in terms of groundwater level (Fig. 18). The trend component curve itself does not show a continuous positive nor negative trend over the whole 30–year period, but rather demonstrates varying trend directions at different periods (Fig. 15c; Fig. 16c; Fig.17c). The seasonal strength of the representative groundwater level is close to that of the air temperature (Fig. 18). The
450 stream flow demonstrates some level of trend and seasonality (Fig. 15e–f; Fig. 16e–f; Fig. 17e–f). The trend and seasonal strengths of the separated baseflow time series are medium, and the different baseflow time series fall somewhere between the stream flow and representative groundwater level (Fig. 18). This indicates that there is a range of outcomes, in terms of trend

and seasonal components, that varies from more similar to the stream flow characteristics to closer to the representative groundwater level characteristics. It seems that the Nathan approach provides baseflow with closer link to the representative groundwater level.
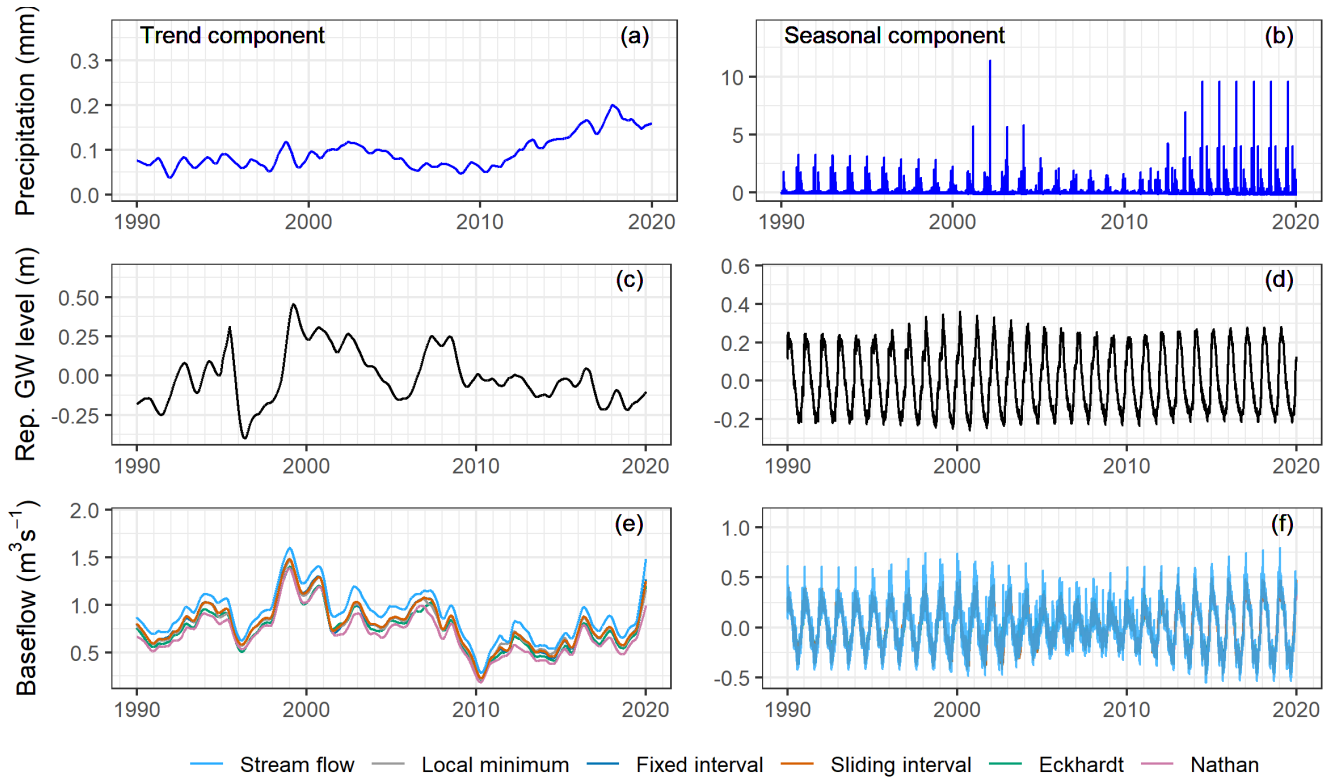
Figure 15 The trend and seasonal components of the decomposed precipitation, representative groundwater level, stream flow and separated baseflow in the Zwarte Beek.
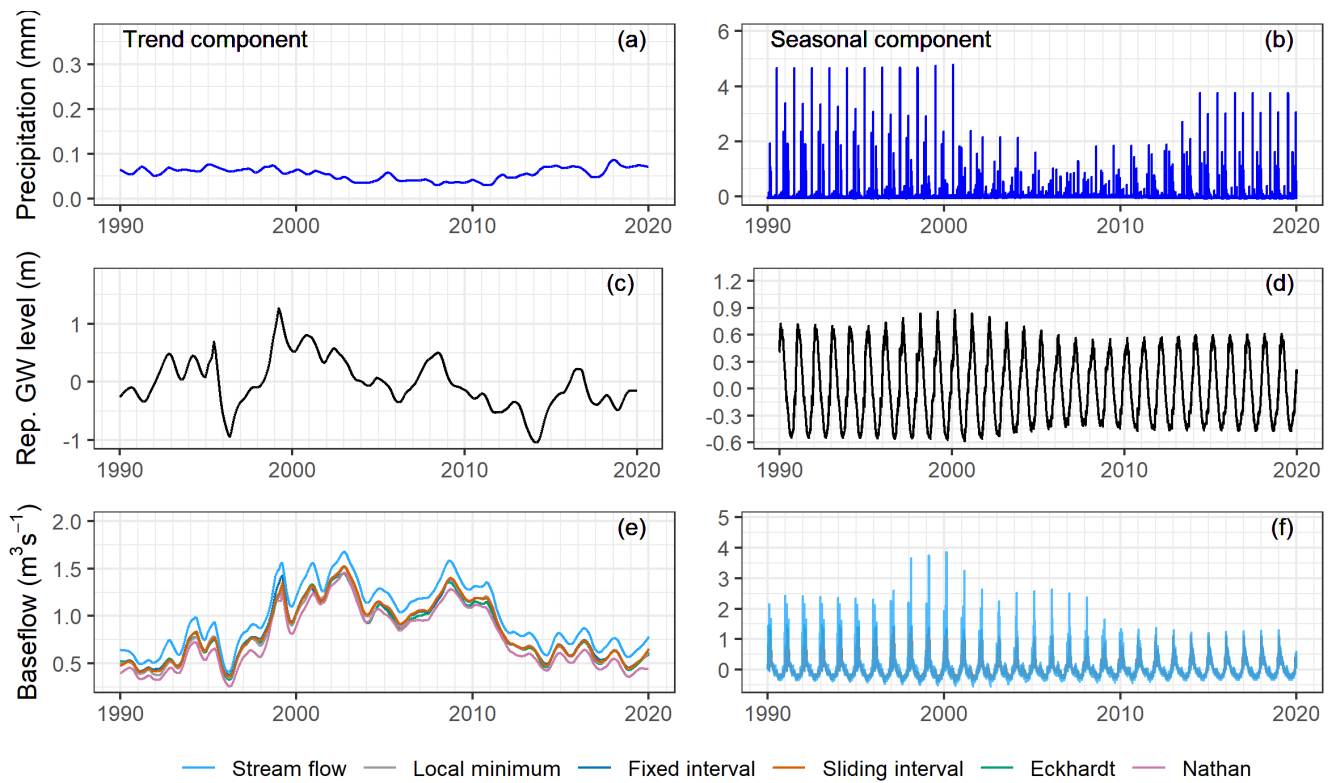
460

Figure 16 The trend and seasonal components of the decomposed precipitation, representative groundwater level, stream flow and separated baseflow in the Herk and Mombeek.
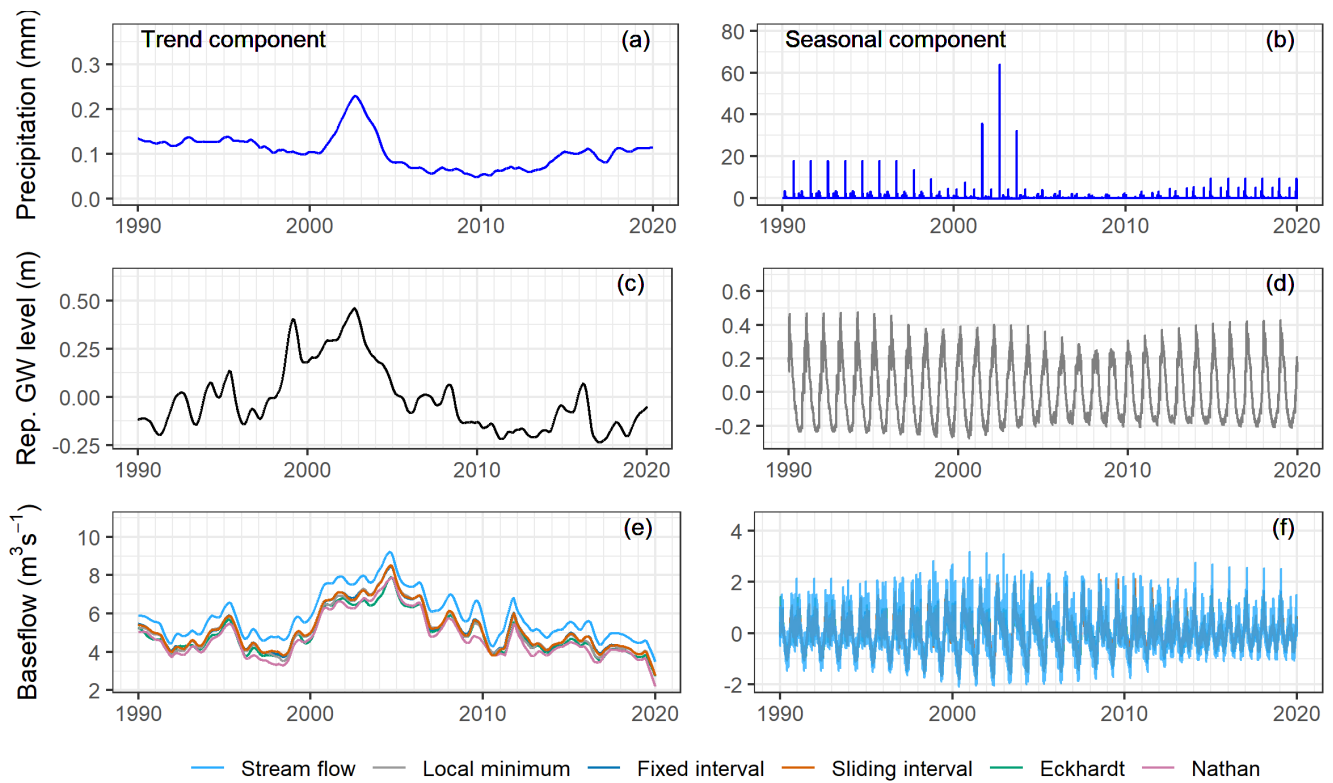
Figure 17 The trend and seasonal components of the decomposed precipitation, representative groundwater level, stream flow and separated baseflow in the Dijle.
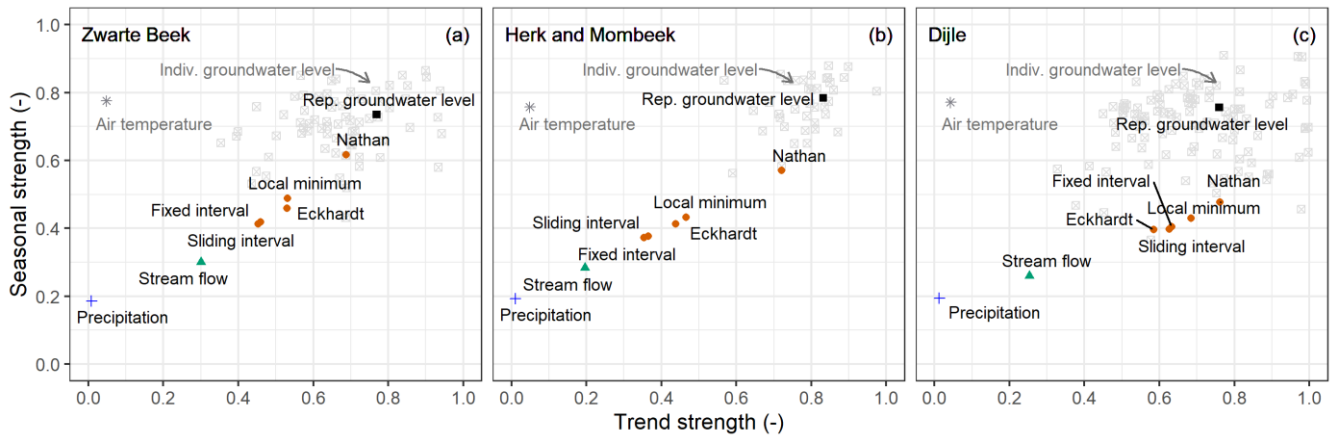
Figure 18 Trend and seasonal strengths of the precipitation, air temperature, representative groundwater level, individual groundwater level, stream flow and separated baseflow in the three catchments.

5 Discussion

5.1 Baseflow and groundwater inflow estimation

As important indicators of river–aquifer interactions, baseflow is estimated here from the stream flow record, and the groundwater inflow to rivers is estimated based on groundwater level. The latter approach does still rely on the first however, as separated baseflow is used as the dependent variable in the modelling exercise.

Baseflow separation is a subjective process which is based on different mathematical techniques rather than the physical processes governing river–aquifer exchange (Sloto and Crouse, 1996; Batelaan and De Smedt, 2007; Killian et al., 2019). Three methods from HYSEP select the minimum values of the hydrograph with an interval by different algorithms (Sloto and Crouse, 1996). Alternatively, the Nathan and Eckhardt methods use parameters which have some physical connection with the catchment characteristics, such as flow status of streams within the year (perennial or ephemeral) and the permeability of the aquifers (Nathan and McMahon, 1990; Arnold and Allen, 1999; Eckhardt, 2005).

Despite the methodological differences, the mean BFIs of the separated baseflow time series are never less than 0.70 in the three catchments (Fig. 5–7). These high BFIs indicate that the studied catchments are groundwater–dominated lowland catchments, which is also reflected in the flat slope of the FDCs (Fig. 3a). The mean BFI ranges of the three catchments agree well with the previous study by Batelaan and De Smedt (2007), where the range are 0.81–0.83 for the Zwarte Beek, 0.79–0.81 for the Demer (the Herk and Mombeek is part of Demer) and 0.81–0.87 for the Dijle, using the Slote and Crouse method (Sloto and Crouse, 1996). In our study, the Eckhardt and Nathan methods generate relatively smooth baseflow time series when compared to the graphical HYSEP methods (Fig. 5–7). Zomlot et al. (2015) conducted baseflow separation in 11 selected regional catchments in Flanders and also found that the one– or two–parameter recursive digital filter methods generated slightly lower mean BFIs than the local minimum method from HYSEP.

Estimated groundwater inflow time series through impulse response modelling, can capture part of the variation of the separated baseflow, but are not reproducing very well the peaks in the separated baseflow. This is consistent with the fact that the separated baseflow from hydrographs is actually the total baseflow, which includes groundwater inflow but also other slower–moving water that sustains stream flow between rainfall events. The difference between the separated baseflow and obtained groundwater inflow can roughly be seen as the delayed water release from other storages other than that in the aquifer. In this context, the impulse response modelling approach from the groundwater flow perspective can allow estimating the groundwater inflow to the river and separating it from the total baseflow.

5.2 Impulse response modelling of the hydrological system

To the best of our knowledge, this is the first study that has used a two–step approach with lumped parameter impulse response modelling for estimating groundwater inflow to rivers in a temperate lowland hydrological system.

For the groundwater level response modelling process, the lowland aquifers react rather fast to the system input. A large number of wells reach their peak response during the first day in the three catchments. For the sake of comparison, we give the response time in groundwater level due to precipitation recharge, estimated in another study (Gonzales et al., 2009) using the impulse response functions by Ventis (Venetic, 1970) and Olsthoorn (Olsthoorn, 2007). A confined coarse sandy aquifer in a Dutch lowland catchment, with an average length of 800 m and thickness of 10 m, a hydraulic conductivity of 30 m d^{-1} and a storability of 1.37×10^{-3} m m^{-1} (Saliha A. H. and Nonner, 2004), has a groundwater response delay of approximately 16 h (0.67 d) for a precipitation event of around 8 mm (Gonzales et al., 2009). This is consistent with the fast response behavior of most wells in our simulations, with peak response during the first day. Since the time step of our model is daily, we thus are not able to capture peak response time shorter than a day. If the model input and level observation time series have higher resolution, the peak response time will probably be less than one day, especially for the shallow unconfined lowland aquifers.

In the Herk and Mombeek, we observed the tendency of faster and higher peak response when the well was closer to the river and the groundwater depth shallower to the surface. As the majority of the groundwater level wells closer to the striped alluvial clay sediment along the river, we saw an impact of the sediment materials on the impulse response. When rainfall events occur, a shallow well close to the river experiences some buffering effect from the clayey sediment in the floodplain close to the river, which delays the process of the activated groundwater to flow fast towards the river. This can lead to a faster and higher response on the near–river groundwater level.

During the groundwater inflow response modelling, the system response is fast and linear. As mentioned before, estimating groundwater inflow from a groundwater perspective can be a promising option. Further research is however recommended to improve the simulation. When extracting the first principle components from the simulated groundwater level time series, more weight can be assigned to wells located close to the river and less weight given to wells afar, for instance, since shallow groundwater closer to the river tends to follow local pathways and brings more contribution to the river. This makes the generated groundwater level more representative for the near-river status. A second improvement can be made in the model itself. Instead of using a constant drainage level, dynamic drainage level time series could for instance be included by adjusting relevant input codes.

5.3 Time series analysis

Although there are several observed drought events in Europe in recent years (e.g. 1992, 2003, 2015 and 2018) (Hänsel et al., 2019; Fu et al., 2020), and our annual precipitation time series show low levels for some years in Belgium (e.g. 1996, 2003, 2013 and 2018), the precipitation trend is still small over the observation window of 30 years. Under temperate humid climates, the precipitation has some seasonal variations but not strong. On the contrary, the trend and seasonality of the groundwater level time series are pronounced. This is due to the strong seasonal impacts from air temperature, which heavily influences the evapotranspiration process in the unsaturated zone. When the precipitation recharge reaches the shallow aquifer, the groundwater level time series inherits similar seasonal patterns from air temperature. Thus, we observe strong seasonality of the representative groundwater level time series.

The trend and seasonal strengths of the stream flow lay between the two ends of precipitation and groundwater level (Fig. 18), which agrees with the fact that stream flow is the end-product of the combined influences from groundwater inflow, precipitation and other flow components. We also observe that the groundwater inflow to rivers is a process where the groundwater (in terms of the representative groundwater level) with strong trend and seasonal signals contributes to the stream flow where the signal is destroyed by the quick flow component, resulting in a weak trend and seasonality (Fig. 18). From the groundwater inflow response modelling perspective, the groundwater inflow to rivers is a fast process and it tends to carry relatively strong trend and seasonal strengths from the groundwater and contributes to the total baseflow. The differences in trend and seasonality strengths of the baseflow and groundwater level are the influences of other delayed sources contributing to baseflow. Since the trend and seasonality of the baseflow from the Nathan method closer to those of the groundwater level, it is more in line with the groundwater inflow from the groundwater-level-based approach, and may be the best baseflow separation method to estimate groundwater inflow in this context.

6 Conclusions

Through a combined approach of baseflow separation, impulse response modelling and time series analysis, we gained better insights into the river-aquifer interactions and the lowland hydrological system in the three catchments.

The graphical HYSEP (fixed interval, sliding interval and local minimum) and recursive digital filter approaches (Nathan and Eckhardt) yield high mean BFIs (≥ 0.70), indicating a strong groundwater–dominated feature in the study area. The recursive digital filter methods generate a relatively smoother baseflow time series than the graphical HYSEP ones.

We explored the lowland hydrological system with impulse response modelling in two steps, (1) the groundwater level response to system input of precipitation and air temperature, and (2) the groundwater inflow response to system input of groundwater level. For the first process, groundwater level in shallow aquifers reacts fast to the system input, with most of the

wells reaching their peak response during the first day. There is an overall trend of faster response time and higher response magnitude in the wet than the dry periods in the study areas. In the Herk and Mombeek, the stream bed and bank consist of clay materials, which have some buffering effects for the near–river hydraulic interactions. Thus, there is a tendency of faster
565 peak time and higher peak response when the well is closer to the river and the groundwater depth shallower to the surface.

During the second process, the system response is fast and the simulated groundwater inflow can capture some variations but not the peaks of the separated baseflow. The differences between the separated baseflow and the simulated groundwater inflow is delayed water release from other intermediate storages. As the groundwater inflow estimation from the groundwater
570 perspective considers to some level the physical connection between river and aquifer in the subsurface, it can be an alternative method to assess the groundwater contribution to rivers.

The trend and seasonality analysis of the time series shows that the groundwater inflow to rivers is a process where the strong trend and seasonal characteristics of the groundwater level are intervened by the quick flow component resulting in stream
575 flow with a weak trend and seasonality. By comparing strengths of the decomposed components, the Nathan approach seems to provide baseflow estimates that are closer related to groundwater inflow in this lowland setting.

Based the performances of the combined approach in our study sites, we consider this approach has further potential to be applied to similar lowland catchments with small area coverages and under natural conditions or limited human impacts.

580 **Code availability**

The RRAWFLOW code is publicly available at https://www.usgs.gov/centers/dakota-water/science/rrawflow-rainfall-response-aquifer-and-watershed-flow-model?qt-science_center_objects=7#qt-science_center_objects (Long, 2015). R functions from DVstats (Lorenz, 2017), EcoHydRology (DR et al., 2018) and FlowScreen (Dierauer and Whitfield, 2019) packages are available for baseflow separation using HYSEP, Nathan and Eckhardt methods, respectively.

585 **Data availability**

Meteorological input data (precipitation and air temperature) were obtained on request from KMI (Koninklijk Meteorologisch Instituut). Stream flow data are available at https://www.waterinfo.be and downloaded via the wateRinfo R package interface (Van Hoey, 2020). All groundwater data are available via the web services of INBO (Instituut voor Natuur- en Bosonderzoek), DOV (Databank Ondergrond Vlaanderen) and DEE (Département de l'Environnement et de l'Eau).

Author contribution

ML and BR conceived and designed the study. ML conducted the analyses under the mentorship of BR. ML wrote the manuscript. All authors took part in the discussion of the results and revisions of the manuscript.

Competing interests

The authors declare that they have no conflict of interest.

Financial support

Funding for this study was provided by the Fonds Wetenschappelijk Onderzoek in Flanders, Belgium, under grant agreement Nr. S003017N – Future Floodplains: ecosystem services of floodplains under socio-ecological change. The article processing charges for this open-access were covered by KU Leuven.

Review statement

This paper was edited by Nadia Ursino and reviewed by Franklin Schwartz and one anonymous referee.

References

Alaghmand, S., Beecham, S., Woods, J. A., Holland, K. L., Jolly, I. D., Hassanli, A., and Nouri, H.: Quantifying the impacts of artificial flooding as a salt interception measure on a river-floodplain interaction in a semi-arid saline floodplain, Environ. Modell. Softw.,79, 167–183, https://doi.org/10.1016/j.envsoft.2016.02.006, 2016.

Anibas, C., Fleckenstein, J. H., Volze, N., Buis, K., Verhoeven, R., Meire, P., and Batelaan, O.: Transient or steady-state? Using vertical temperature profiles to quantify groundwater-surface water exchange, Hydrol. Process., 23, 2165–2177, https://doi.org/10.1002/hyp.7289, 2009.

Anibas, C., Buis, K., Verhoeven, R., Meire, P., and Batelaan, O.: A simple thermal mapping method for seasonal spatial patterns of groundwater–surface water interaction, J. Hydrol., 397, 93–104, https://doi.org/10.1016/j.jhydrol.2010.11.036, 2011.

Anibas, C., Schneidewind, U., Vandersteen, G., Joris, I., Seuntjens, P., and Batelaan, O.: From streambed temperature measurements to spatial-temporal flux quantification: Using the LPML method to study groundwater-surface water interaction, Hydrol. Process., 30, 203–216, https://doi.org/10.1002/hyp.10588, 2015.

Anibas, C., Tolche, A. D., Ghysels, G., Nossent, J., Schneidewind, U., Huysmans, M., and Batelaan, O.: Delineation of spatial-temporal patterns of groundwater/surface-water interaction along a river reach (Aa river, belgium) with transient thermal modeling, Hydrogeol. J., 26, 819–835, https://doi.org/10.1007/s10040-017-1695-9, 2017.

Arnold, J. G. and Allen, P. M.: Automated methods for estimating baseflow and ground water recharge from streamflow records, J. Am. Water Resour. As., 35, 411–424, https://doi.org/10.1111/j.1752-1688.1999.tb03599.x, 1999.

Asmuth, J. R. von and Knotters, M.: Characterising groundwater dynamics based on a system identification approach, J. Hydrol., 296, 118–134, https://doi.org/10.1016/j.jhydrol.2004.03.015, 2004.

Asmuth, J. R. von, Bierkens, M. F. P., and Maas, K.: Transfer function-noise modeling in continuous time using predefined impulse response functions, Water Resour. Res., 38, 23–1–23–12, https://doi.org/10.1029/2001wr001136, 2002.

Barthel, R. and Banzhaf, S.: Groundwater and surface water interaction at the regional-scale a review with focus on regional integrated models, Water Resour. Manag., 30, 1–32, https://doi.org/10.1007/s11269-015-1163-z, 2016.

Batelaan, O. and De Smedt, F.: GIS-based recharge estimation by coupling surface–subsurface water balances, J. Hydrol., 337, 337–355, https://doi.org/10.1016/j.jhydrol.2007.02.001, 2007.

Brunner, P., Therrien, R., Renard, P., Simmons, C. T., and Franssen, H.-J. H.: Advances in understanding river-groundwater interactions, Rev. Geophys., 55, 818–854, https://doi.org/10.1002/2017rg000556, 2017.

Byrd, R. H., Lu, P., Nocedal, J., and Zhu, C.: A limited memory algorithm for bound constrained optimization, SIAM J. Sci. Comput., 16, 1190–1208, https://doi.org/10.1137/0916069, 1995.

Cleveland, R. B., Cleveland, W. S., McRae, J. E., and Terpenning, I.: STL: A seasonal-trend decomposition, J. Off. Stat., 6, 3–73, 1990.

Cushman, J. H. and Tartakovsky, D. M. (Eds.): The Handbook of Groundwater Engineering (3rd ed.), CRC Press, Boca Raton, United States, https://doi.org/10.1201/9781315371801, 2016.

Di Ciacca, A., Leterme, B., Laloy, E., Jacques, D., and Vanderborght, J.: Scale-dependent parameterization of groundwater–surface water interactions in a regional hydrogeological model, J. Hydrol., 576, 494–507, https://doi.org/10.1016/j.jhydrol.2019.06.072, 2019.

Dierauer, J. and Whitfield, P.: FlowScreen: Daily streamflow trend and change point screening, 2019.

DOV: Databank Ondergrond Vlaanderen (Flanders Subsurface Database), http://www.dov.vlaanderen.be, last access: 1 Jan., 2020.

DR, F., MT, W., JA, A., TS, S., and ZM, E.: EcoHydRology: A community modeling foundation for eco-hydrology, 2018.

Eckhardt, K.: How to construct recursive digital filters for baseflow separation, Hydrol. Process., 19, 507–515, https://doi.org/10.1002/hyp.5675, 2005.

Eckhardt, K.: A comparison of baseflow indices, which were calculated with seven different baseflow separation methods, J. Hydrol., 352, 168–173, https://doi.org/10.1016/j.jhydrol.2008.01.005, 2008.

Fan, J. and Gijbels, I.: Local Polynomial Modelling and its Applications (1st ed.), Routledge, Boca Raton, United States, https://doi.org/10.1201/9780203748725, 2018.

Fu, Z., Ciais, P., Bastos, A., Stoy, P. C., Yang, H., Green, J. K., Wang, B., Yu, K., Huang, Y., Knohl, A., and others: Sensitivity of gross primary productivity to climatic drivers during the summer drought of 2018 in Europe, Phil. Trans. R. Soc. B, 375,

650   20190747, https://doi.org/10.1098/rstb.2019.0747, 2020.

Ghysels, G., Benoit, S., Awol, H., Jensen, E. P., Tolche, A. D., Anibas, C., and Huysmans, M.: Characterization of meter-scale spatial variability of riverbed hydraulic conductivity in a lowland river (Aa river, Belgium), J. Hydrol., 559, 1013–1027, https://doi.org/10.1016/j.jhydrol.2018.03.002, 2018.

Ghysels, G., Anibas, C., Awol, H., Tolche, A. D., Schneidewind, U., and Huysmans, M.: The significance of vertical and

655   lateral groundwaterSurface water exchange fluxes in riverbeds and riverbanks: Comparing 1D analytical flux estimates with 3D groundwater modelling, Water, 13, 306, https://doi.org/10.3390/w13030306, 2021.

Gonzales, A. L., Nonner, J., Heijkers, J., and Uhlenbrook, S.: Comparison of different base flow separation methods in a lowland catchment, Hydrol. Earth Syst. Sci., 13, 2055–2068, https://doi.org/10.5194/hess-13-2055-2009, 2009.

Hall, F. R.: Base-flow recessions-a review, Water Resour. Res., 4, 973–983, https://doi.org/10.1029/wr004i005p00973, 1968.

660   Hänsel, S., Ustrnul, Z., Łupikasza, E., and Skalak, P.: Assessing seasonal drought variations and trends over Central Europe, Adv. Water Resour., 127, 53–75, https://doi.org/10.1016/j.advwatres.2019.03.005, 2019.

Hyndman, R. J. and Athanasopoulos, G.: Forecasting: principles and practice (3rd ed.), OTexts, Melbourne, Australia, https://otexts.com/fpp3/, last access: 1 Dec., 2021.

Jakeman, A. J. and Hornberger, G. M.: How much complexity is warranted in a rainfall–runoff model?, Water Resour. Res.,

665   29, 2637–2649, https://doi.org/10.1029/93wr00877, 1993.

Killian, C. D., Asquith, W. H., Barlow, J. R. B., Bent, G. C., Kress, W. H., Barlow, P. M., and Schmitz, D. W.: Characterizing groundwater and surface-water interaction using hydrograph-separation techniques and groundwater-level data throughout the Mississippi Delta, USA, Hydrogeol. J., 27, 2167–2179, https://doi.org/10.1007/s10040-019-01981-6, 2019.

KMI: Koninklijk Meteorologisch Instituut (Royal Meteorological Institute), http://www.kmi.be, last access: 1 Jan., 2020.

670   Krause, S., Blume, T., and Cassidy, N. J.: Investigating patterns and controls of groundwater up-welling in a lowland river by combining Fibre-optic Distributed Temperature Sensing with observations of vertical hydraulic gradients, Hydrol. Earth Syst. Sci., 16, 1775–1792, https://doi.org/10.5194/hess-16-1775-2012, 2012.

Laaha, G., Gauster, T., Tallaksen, L. M., Vidal, J.-P., Stahl, K., Prudhomme, C., Heudorfer, B., Vlnas, R., Ionita, M., Van Lanen, H. A., and others: The European 2015 drought from a hydrological perspective, Hydrol. Earth Syst. Sci., 21, 3001–

675   3024, https://doi.org/10.5194/hess-21-3001-2017, 2017.

Laga, P., Louwye, S., and Geets, S.: Paleogene and Neogene lithostratigraphic units (Belgium), Geol. Belg., 4, 135-152, https://doi.org/10.20341/gb.2014.050, 2001.

Long, A. J.: RRAWFLOW: Rainfall-response aquifer and watershed flow model (v1.15), Geosci. Model Dev., 8, 865–880, https://doi.org/10.5194/gmd-8-865-2015, 2015.

680   Long, A. J. and Mahler, B. J.: Prediction, time variance, and classification of hydraulic response to recharge in two karst aquifers, Hydrol. Earth Syst. Sci., 17, 281–294, https://doi.org/10.5194/hess-17-281-2013, 2013.

Lorenz, D.: DVstats: Functions to manipulate daily-values data, 2017.

Nash, J. E. and Sutcliffe, J. V.: River flow forecasting through conceptual models part i– A discussion of principles, J. Hydrol., 10, 282–290, https://doi.org/10.1016/0022-1694(70)90255-6, 1970.

685 Nathan, R. J. and McMahon, T. A.: Evaluation of automated techniques for base flow and recession analyses, Water Resour. Res., 26, 1465–1473, https://doi.org/10.1029/wr026i007p01465, 1990.

Niswonger, R. G. and Prudic, D. E.: Documentation of the Streamflow-Routing (SFR2) Package to Include Unsaturated Flow Beneath Streams - A Modification to SFR1, U.S. Geological Survey, No. 6-A13, https://doi.org/10.3133/tm6a13, 2005.

Nützmann, G., Levers, C., and Lewandowski, J.: Coupled groundwater flow and heat transport simulation for estimating
690 transient aquifer-stream exchange at the lowland River Spree (Germany), Hydrol. Process., 28, 4078–4090, https://doi.org/10.1002/hyp.9932, 2013.

Olsthoorn, T. N.: Do a bit more with convolution, Groundwater, 46, 13–22, https://doi.org/10.1111/j.1745-6584.2007.00342.x, 2007.

Pearson, K.: Mathematical Contributions to the theory of Evolution. III. Regression, Heredity, and Panmixia, Philos. T. R. Soc.
695 Lond., 187, 253–318, https://doi.org/10.1098/rsta.1896.0007, 1896.

Peterson, R. A. and Cavanaugh, J. E.: Ordered quantile normalization: A semiparametric transformation built for the cross-validation era, J. Appl. Stat., 47, 2312–2327, https://doi.org/10.1080/02664763.2019.1630372, 2019.

Peterson, R. A. and Peterson, M. R. A.: Package "bestNormalize", 27, 2020.

Piggott, A.R., Moin, S. and Southam, C.: A revised approach to the UKIH method for the calculation of baseflow/Une approche
700 améliorée de la méthode de l'UKIH pour le calcul de l'écoulement de base, Hydrolog. Sci. J., 50, 911-920, https://doi.org/10.1623/hysj.2005.50.5.911, 2005.

Poulsen, J. R., Sebok, E., Duque, C., Tetzlaff, D., and Engesgaard, P. K.: Detecting groundwater discharge dynamics from point-to-catchment scale in a lowland stream: Combining hydraulic and tracer methods, Hydrol. Earth Syst. Sci., 19, 1871–1886, https://doi.org/10.5194/hess-19-1871-2015, 2015.

705 Rutledge, A. T.: Computer programs for describing the recession of ground-water discharge and for estimating mean ground-water recharge and discharge from streamflow records: Update, U.S. Department of the Interior, U.S. Geological Survey, No. 98-4148, https://doi.org/10.3133/wri984148, 1998.

Saliha A. H., J., Zhengyue and Nonner, J.: Modelling the Western Betuwe Area. Water Science and Engineering–Hydrology and Water Resources, Master's thesis, International Institute for Infrastructural, Hydraulic; Environmental Engineering – IHE,
710 Delft, The Netherlands, 2004.

Schneidewind, U., Berkel, M. van, Anibas, C., Vandersteen, G., Schmidt, C., Joris, I., Seuntjens, P., Batelaan, O., and Zwart, H. J.: LPMLE3: A novel 1-D approach to study water flow in streambeds using heat as a tracer, Water Resour. Res., 52, 6596–6610, https://doi.org/10.1002/2015wr017453, 2016.

Searcy, J. K.: Flow-duration curves, U.S. Government Printing Office, 1959.

715   Sloto, R. A. and Crouse, M. Y.: HYSEP: A computer program for streamflow hydrograph separation and analysis, U.S. Geological Survey, No. 96-4040, https://doi.org/10.3133/wri964040, 1996.

Spinoni, J., Vogt, J. V., Naumann, G., Barbosa, P., and Dosio, A.: Will drought events become more frequent and severe in Europe?, Int. J. Climatol., 38, 1718–1736, https://doi.org/10.1002/joc.5291, 2017.

Tallaksen, L. M. and Van Lanen, H. A. (Eds.): Hydrological drought: Processes and estimation methods for streamflow and
720   groundwater (1st ed.), Elsevier, 2004.

Turkelboom, F., Demeyer, R., Vranken, L. et al. How does a nature-based solution for flood control compare to a technical solution? Case study evidence from Belgium. Ambio 50, 1431–1445, https://doi.org/10.1007/s13280-021-01548-4, 2021.

Van Hoey, S.: WateRinfo: Download time series data from waterinfo.be, 2020.

Van Walsum, P. E. V., Verdonschot, P. F. M., and Runhaar, J.: Effects of climate and land-use change on lowland stream
725   ecosystems, No. 523, Alterra, 2002.

Venetic, C.: Finite aquifers: Characteristic responses and applications, J. Hydrol., 12, 53–62, https://doi.org/10.1016/0022-1694(70)90032-6, 1970.

Vogel, R. M. and Fennessey, N. M.: Flow-duration curves. I: New interpretation and confidence intervals, J. Water Res. Plan Man., 120, 485–504, https://doi.org/10.1061/(asce)0733-9496(1994)120:4(485), 1994.

730   Young, P. C.: Hypothetico-inductive data-based mechanistic modeling of hydrological systems, Water Resour. Res., 49, 915–935, https://doi.org/10.1002/wrcr.20068, 2013.

Zomlot, Z., Verbeiren, B., Huysmans, M., and Batelaan, O.: Spatial distribution of groundwater recharge and base flow: Assessment of controlling factors, J. Hydrol. Reg. Stud., 4, 349–368, https://doi.org/10.1016/j.ejrh.2015.07.005, 2015.